PNC TN9410 96-068

公開資料

Order of Magnitude Analysis of Stratified Natural Convection and Mixed Convection Penetration Flow of Cold Liquid into a Vertical Channel with Hot, Forced Flow

MAY, 1996

OARAI ENGINEERING CENTER
POWER REACTOR AND NUCLEAR FUEL DEVELOPMENT CORPORATION

動力炉・核燃料開発事業団
(Power Reactor and Nuclear Fuel Development Corporation) 1996

Order of Magnitude Analysis of Stratified Natural Convection and Mixed Convection Penetration Flow of Cold Liquid into a Vertical Channel with Hot, Forced Flow

MAY, 1996

OARAI ENGINEERING CENTER
POWER REACTOR AND NUCLEAR FUEL DEVELOPMENT CORPORATION

PNC TN9410 96-068
March, 1996

Order of Magnitude Analysis of stratified natural convection and mixed convection penetration flow of cold liquid into a vertical channel with hot, forced flow

A. Tokuhiro*1 and J. Kobayashi*1

Abstract

In the thermal-hydraulic analysis of nuclear reactors and other energy-related systems, the proper scaling of simulation experiments and separate effect studies, is first determined by the identification of the relevant dimensionless group(s) and then by the reproduction in magnitude of the range. While most experiments contain some idealizations in geometry so that well-known dimensionless groups can be easily identified, the non-ideal nature of any given experiment may appear for instance, in the presentation of data using the selected dimensionless numbers. If this is the case, a reconsideration of the Scale Analysis or Order of Magnitude Analysis (OMA) may reveal slight modifications to classic results that originate from ideal cases. The present work summarizes OMA by way of example; that is, a reconsideration of the stratified natural convection problem from which a stratified Nusselt number is introduced. Two data sets are presented in support of the described modification.

This is then followed by an experimental investigation on penetration of cold liquid into a modeled subassembly channel under mixed convection, from the hot plenum of a protypical FBR design. The penetration phenomenon occurs under certain natural circulation conditions during the operation of the DRACS (direct reactor auxiliary cooling system) for decay heat removal and can influence the natural circulation head that determines the core flow rate and consequently the core cooling rate. In the present experiment, a simplified test section simulating the upper plenum and a subassembly channel was constructed wherein both temperature and velocity measurements were made to investigate the penetration of cold water into a vertical channel with upward flowing hot water. Upon comparing temperature and velocity data we found an overall similarity in their respective spatio-temporal distributions as expected. The data suggested correlations describing the onset of flow penetration and penetration depth into the channel, expressed not only by the Richardson number (= Gr/Re^2), but including the Prandtl number and aspect ratio of the channel. This result was deduced from OMA after using the Ri-number alone indicated that a reconsideration was in store.

---

*1 Reactor Engineering Section

公　開　資　料
PNC TN9410 96-068
１９９６年３月

燃料集合体入口チャンネル高温強制対流への低温流体の混合対流潜り込み流れの支配パラメータ次元解析

A. Tokuhiro *、小林　順*

要旨

高速炉を模擬した上部プレナムから燃料集合体への低温流体の混合対流潜り込み流れの実験研究が行われた。この潜り込み現象は、ＤＲＡＣＳ（direct reactor auxiliary cooling system）を使用した自然循環による崩壊熱除去時のある条件下において発生し、炉心流量を決定する自然循環ヘッドと炉心の冷却性に影響を与える可能性がある。本試験では、上部プレナムと燃料集合体入口チャンネルを単純化した試験体を用いて、垂直チャンネル内の高温上昇流へ低温流体が潜り込む現象に対して、瞬間的な温度分布と流速分布の計測を行った。その結果、瞬間的な温度分布および流速分布の時間変化はほぼ同一であることが確認された。得られた実験データにより、潜り込みの初生条件とチャンネルへの潜り込み深さを、与えられたＰｒ数に対してＲｅ数とＧｒ数の組み合わせで表すことに成功した。潜り込み現象は温度および流速データによって判断した。本報告では、得られた結果が他の同様な研究と若干の違いがあるが、実験データを充分に取り入れた次元解析に基づいた無次元数の組み合わせを提案する。

大洗工学センター　安全工学部　原子炉工学室

Contents

List of Tables

List of Figures

I. Introduction

Forced convection, natural convection, mixed convection and thermal stratfication are recurring themes in convective heat transfer or thermal-hydraulics of nuclear reactors and many other energy-related systems. In particular, as a matter of design or analysis related to safety issues, both numerical and experimental investigations on convective heat transfer are usually conducted. In such circumstances, the proper scaling and modeling of relevant variables may heavily influence the outcome of the study. Specifically, in an experimental study the proper scaling (geometrically) and simulation (phenomenologically) is essential if the results are to be extrapolated to the real system. We know that in order to properly simulate the thermal-hydraulics in an experiment, we first need to identify the relevant dimensionless group(s) and then reproduce in magnitude the range of these groups. While most experiments contain some idealizations in geometry so that well-known dimensionless groups can be easily identified, there may be a non-ideal aspect contained as well. As a consequence of some non-ideal nature of a given experiment, the presentation of data using the identified groups may exhibit a degree of scatter in the datum points deemed unsatisfactory. When this occurs, one of the easily available courses of action is a reconsideration of the identified dimensionless groups. It may be for instance, that mixed convection is of more relevance in the experiment than natural convection, which was at first assumed. If this were the case, plotting the heat transfer by using the Nu-number versus the Gr-number, would certainly reveal a departure of the experimental points from the accepted natural convection correlation. In these instances then a Scale Analysis or Order of Magnitude Analysis (OMA) may reveal slight modifications to the classic results that often originate from highly ideal (and often experimentally unrealizable) cases.

In the present report we will consider by way of example OMA as a simple analytical tool with which to account for some of the non-idealness of experimental systems. Since one of the most common non-ideal aspects is that of a finite, instead of an infinite volume, in natural convection of finite volumes, thermal stratification is a common occurrence. In order to thus introduce OMA, a consideration of the *stratified* natural convection problem from which we derive a *stratified* Nusselt number is given. That this approach is apparently correct is given by application to two available data sets.

Subsequently, we report on an experiment where we are interested in the penetrating flow of buoyancy-driven cold liquid (water) into a forcibly-driven, upward flow of hot liquid in a vertical channel. The test facility simulates and is of relevance to the thermal-hydraulics of an inlet channel (subassembly) connected to an upper hot plenum of a LMFBR. Results from flow visualization studies and quantitative temperature and Laser Doppler Anemometry (LDA) velocity measurments revealed certain aspects of the penetrating flow phenomenon. We additionally supplemented LDA measurements with ultrasound Doppler velocimetry measurements, focusing especially on the penetrating flow. Cumulatively, we then derived a

criterion for penetrating flow and a correlation describing the penetration *depth* based intially on the accepted mixed convection dimensionless group, the Richardson number (= Gr/Re^2). The degree of scatter in the data however revealed a need to reconsider the appropriatenesss of the Ri-number. A simple OMA type analysis revealed some *fine tuning*. These results will be presented in this work.

II. Order of Magnitude Analysis

Order of Magnitude Analysis (OMA) is a common sense approach to thermal-hydraulic analysis, whether this be in relation to a numerical or experimental study. If you have ever heard of the term "back of the envelope calculation", you can be certain that many times OMA has been used. It is not to be confused with *dimensional analysis* which is based on Buckingham's π-Theorem. This technique is based on guessing the relevant physical parameters (i.e. ν, ρ, κ etc.), noting their dimensions and systematically following a set of rules to derive a dimensionless parameter. If one omits a relevant parameter, then that parameter is simply excluded from any resulting dimensionless group. It can however, be used effectively if precautions are taken. OMA is also not to be mistaken with the non-dimensionalization of the governing equations which is a method to those unfamiliar, that often appears arbitrary and "conducted randomly". A OMA-type analysis should be done before non-dimensionalizing the governing equations, but this fact is unfortunately overlook most of the time. On the other hand, OMA often begins with the conservation equations and compares terms so that they can either be retained or discarded from the analysis, based on physical arguments.

II. 1 Introduction and guidelines

As an introduction, we first outline some guidelines to follow when applying OMA or Scale Analysis to your problem of interest. These "rules" closely follow the description by Bejan [1; pp. 19-20].

1) If you can define the spatial extent of the region in which you perform the scale analysis; that is, if you know as fact or can measure a length within the region of interest, take this as the *length scale*. Often this may be the diameter of a pipe (D) , a length of a pipe (L) or the height and width of a rectangular enclosure (H,W). It is possible that there are more than one obvious length scales (as in H, W). However, it is also possible to specify an unknown length scale, such as the boundary layer thickness δ in boundary layer flow, when one knows, although not absolutely necessary, *apriori* (before performing the analysis) that such a boundary layer exists and is of direct relevance to the problem at hand. This means in effect that

the flow changes *significantly* or the convective heat transfer takes place *across* (i.e. from wall to fluid) respectively, a hydrodynamic or thermal boundary layer.

2) The balance equations which one writes are algebraic equivalence equations of the governing equations (mass, momentum and energy) and constitutive relationships, which may already be in equality form, such as the ideal gas law (pV = nRT). The accepted mathematical symbol use for equivalence is "~" and in comparison to differential equations, integral or differential-integral equations most commonly seen in engineering algebraic equivalence relationships are considered "zero-eth" order (or equations) or dimensionless. As for the equivalence itself, it describes the *equivalence* (or balance) between the scales (or magnitude) of two dominant terms appearing in the relationship. What are these *dominant* terms? They are usually terms that describe for example the buoyancy or inertial forces in natural convection (in the momentum equation) or thermal diffusivity term [α (d^2T/dx^2)] in the energy equation; there may be more than one per "side" of the relationship. The selection of dominant scales is determined as follows.

3) If in the sum of two terms $c = a + b$, the order of magnitude of one term is greater than the other (*apriori* knowledge may help here) ; that is, if $O(a) > O(b)$, then the order of the sum is dictated by the dominant term. This holds true for $c = a - b$ as well. So, we then have $O(c) \sim O(a)$ as our equivalence realtionship.

4) If the sum of two terms are of the same order of magnitude, then the sume is also the same order of magnitude. Thus, if $O(a) \sim O(b)$, then $O(a) \sim O(b) \sim O(c)$.

5) In any product, the order of magnitude of the product is equal to the product of the order fo magnitude of the two factors; that is; if $p = ab$, then $O(p) \sim O(a)O(b)$. Similarly, if $r = a/b$, then $O(r) \sim O(a)/O(b)$.

II. 1 Example: Transient 1D heat conduction

Let us apply this to a very simple example of a heated (or cooled) slab of metal at temperature T_0, that at time t=0 is immersed into a cold (or hot), *highly-conducting* liquid. Assume that the plate's outer surface temperature instantaneously assumes the fluid temperature, T_∞. So, how much time does it take for the half-thickness of the plate, say D/2, to "realize" the influence of T_∞ ? Approach this from a one-dimensional pure conduction problem, for which the energy equation is,

$$\rho C_p (\partial T/\partial t) = \kappa (\partial^2 T/\partial y^2) \qquad \textit{(Eq. a)}$$

Since *apriori* we know that eventually the plate reaches T_∞, there is a characteristic $\Delta T = T_0 - T_\infty$, a half-thickness D/2 and some time variable, t, which is unknown. When we estimate the order of magnitude of the terms in Eq. 1, we use these characteristic parameters and *transform* the differential equation into an algebraic one.

So, the time-dependent term and conduction term are respectively,

$$\rho C_p (\partial T / \partial t) \sim \rho C_p \Delta T / t \qquad \textit{(Eq. b)}$$

and

$$\kappa (\partial^2 T / \partial y^2) \sim \kappa (\partial/\partial y)(\partial T/\partial y)) \sim \kappa \Delta T / (D/2)^2 \quad \textit{(Eq. c)}$$

Upon equating Eq. 1b and 1c we arrive, in terms of the time

$$t \sim (D/2)^2 / \alpha \qquad \textit{(Eq. d)}$$

where α is the thermal diffusivity. The time as estimated from Eq. 1d compares well with exact solution which involves Fourier analysis and a graphical presentation of Fourier series.

II.2 Stratification in an infinite volume

Thermal stratification of a body of fluid often occurs when that fluid under considertion is spatially confinec and ther is addtion (or extraction) of heat-energy into (out of) this fluid. Here we assume that the change in the density of the fluid with a change in temperature is negative ($d\rho/dT < 0$). Two examples are rivers which become thermally stratified from the injection of thermal effluents (high-temperature waste liquids) and the stratification of the local atomosphere after a sunny day (the so-called temperature inversion). These phenomena are characterized by the existence of vertical temperature gradients. In large-scale heat transfer systems, where natural convection is the primary heat removal (or addition) mechanism, stratification influences the rate of heat transfer. It is therefore important to understand how stratification influences the heat transfer rate.

The fundamental aspects of buoyancy-induced stratified phenomena have been discussed by Jaluria [2] and Gebhart et al. [3] . In investigating the thermodynamic criteria for stable stratified convection, both Jaluria and Gebhart found that even a small, negative bulk temperature gradient could be supported

supported in a given fluid. Normally, one thinks of a positive temperature gradient. Fo most fluids, with the notable exception of water, betweem 0-4°C, the density decreases with an increase in temperature. With this in mind, analytical slutions of the stratified natural convection problems have benn provided by Cheesewright [4], Eichhorn [5], Yang et al. [6], Takeuchi et al. [7], Fujii et al. [8] and Jaluria and Gebhart [9]. These solutions are based on similarity and non-similarity methods and stipulate that both the wall and bulk temperature variations along the x-axis (along the heated length axis) assume a specific functional form. It is not certain if these temperature variations at the wall and, especially in the bulk, can be experimentally realized.

A measure of the strength of stratification is measured by the stratification parameter S and is defined as

$$S \equiv (T_{top} - T_{bottom}) / (T_{wall} - T_{\infty,x}) \qquad (Eq.\ 1)$$

where T_{top} and T_{bulk} are respectively, the bulk temperature at the top and bottom of the heated lentgh and T_{wall} and $T_{\infty,x}$ are respectively, the wall and bulk temperatures. The bulk temperature variation along the heated plate is noted with a generic subscript "x". Other definitions, other than above have been suggested in the literature. However, all the definitions account for the variation in the bulk temperature change in the vertical direction (parallel to gravity g). Note that when the bulk temperature is isothermal (non-stratified), the S-parameter is zero.

The influence of stratification on natural convection heat transfer has been explained as follows. In order to facilitate the discussion, we refer to **Figure 1** which depict idealized linear temperature gradients typically oserved in thermally stratified systems. In contrast to the non-stratified case or isothermal case, the local ambient temperature to the right of the mean temperature is larger than the isothermal case. Here we base our argument on the mean which we think of as the isothermal case and thelinear profiles as shown in Figure 1. Thus as the temperature gradient becomes steeper, a larger fraction of the local ambient temperature is higher than the mean. This subsequently means that the local thermal buoyancy force which drives the natural convection is smaller because $\Delta T = (T_{wall} - T_{\infty,x})$ is smaller. So, the buoyancy-induced convective velocity is smaller as well. Now, in terms of the boundary layer, a decrease in the characteristic velocity would mean an increase in the boundary layer thickness. This would then decrease the heat transfer coefficient since $h \sim k / \delta$, where k is the thermal conductivity of the heat transfer medium. In the stratified case however, the heat transfer can increased because locally (at a given x-location) colder fluid arrives from below and subsequently the temperature gradient that defines the heat transfer across the thermal boundary layer (and initiates the flow) is steeper. In other words, in natural convection flow we all know that a largely conductive heat transfer must first take place across a thermal boundary layer before a

buoyancy-induced flow initiates and creates its own momentum boundary layer. Although this driving force that is proportional to $\Delta T = (T_{wall} - T_{\infty, x})$ is *on-average* smaller due to thermal stratification, near the heated surface the presence of colder fluid from below steepens the temperature gradient that defines the heat transfer process. So even for a given characteristic velocity, *U*, which *on-average* may be smaller in comparison to the isothermal case, the heat transfer coefficient may be larger due to an increase in the local temperature gradient.

II.3 Analysis

Consider natural convection heat transfer from a vertical plate immersed ina stable, stratified lquid metal bath as shown in **Figure 1.** The coordinate system is taken so that the x-axis is along the plate. The plate is of unit width into the figure along the z-axis. The heated wall in the figure is either held at constant heat flux or at constant temperature. An arbitrary, but stratrified bulk temperature profile is shown adjacent to the vertical plate.

When an Order of Magnitude Analysis of the conservation equations is performed, we have the following for steady-state mass, momentum and energy conservation. From the mass conservation,

$$(\partial u / \partial x) + (\partial v / \partial y) = 0 \qquad \textit{(Eq. 2)}$$

and

$$(U / H) \sim (V / \delta) \qquad \textit{(Eq. 3)}$$

where *U* and *V* are respectively, the characterisitic fluid velocities along the x- and y-axes, while *H* and δ are respectively, the characteristic heated length along the plate and boundary layer thickness.

From the momentum equation,

$$u (\partial u / \partial x) + v (\partial v / \partial y) = g \beta (T_{wall} - T_{\infty, x}) \qquad \textit{(Eq. 4)}$$

and

$$U(U / H) + (U \delta / H) (U / \delta) \sim g \beta (T_{wall} - T_{\infty, x}) \qquad \textit{(Eq. 5)}$$

where β is the coefficient of thermal expansion for the fluid. Note that Eq. 3 has been used in Eq. 5 in order to evaluate ν in Eq. 4. The viscous force term in Eq. 4 has been appropriately neglected for liquid metals and the Boussinesq approximation has been made for the fluid. We note that the bulk temperature, $T_{\infty,x}$, is a function of x as a result of a given (yet unspecified) stratification.

Finally, from the energy equation,

$$u\,(\partial T/\partial x) + v\,(\partial T/\partial y) = \alpha\,(\partial^2 T/\partial y^2) \qquad \textit{(Eq. 6)}$$

and

$$\lambda\, U((T_{top} - T_{bottom})/H) + (U\,\delta/H)\,((T_{wall} - T_{\infty,x})/\delta) \sim \alpha\,((T_{wall} - T_{\infty,x})/\delta^2) \qquad \textit{(Eq. 7)}$$

where δ and λ are respectively, the thermal diffusivity and a free parameter which contrasts the magnitude of the two convective terms in the energy equation. The relative magnitude of the two convective terms in Eq. 7 should be determined from available experimental data.

The terms of particular interest in Eqs.(2)-(7) are the convective terms in the energy equation. In the isothermal case, one considers only one characteristic temperature difference; that is, the one across the boundary layer, $\Delta T = (T_{wall} - T_{\infty,x})$. This then enables one to solve the energy equation for the characteristic velocity U and the momentum equation for the boundary layer thickness, δ, as the two unknowns of the problem. In the stratrified case however, there is an additional temperature difference which describes the vertical temperature difference, which we call ΔT_s. We therefore distinguish between $\Delta T_s = (T_{top} - T_{bottom})$ along the x-axis and ΔT_w (subscript w added for clarity) across the boundary layer (along the y-axis), and of course know that ΔT_s and ΔT_w are related. Subsequently, if we solve Eq. 7 for U, we obtain

$$U \sim (\alpha H/\delta^2)\,(1 + \lambda\,(\Delta T_s/\Delta T_w))^{-1} \qquad \textit{(Eq. 8)}$$

Note here that when there is no stratification, $\lambda = 0$, we have the usual relationship for non-stratified natural convection. Additionally, note that an increase or decrease in the boundary layer thickness has a larger influence on U than the temperature ratio term (the second term).

When we eliminate U in the momentum equation (Eq. 5)), using Eq. (10), we obtain an expression for the ratio, H / δ, which is proportional to the Nusselt number. So Eq. (7) becomes,

$$H/\delta \sim (g\beta \Delta T_w H^3/\alpha^2)^{1/4}(1+\lambda(\Delta T_s/\Delta T_w))^{1/2} \qquad \textit{(Eq. 9)}$$

for a wall held at uniform temperature. For uniform heat flux at the wall,

$$H/\delta \sim (g\beta q" H^4/\alpha^2\kappa)^{1/5}(1+\lambda(H/\delta)(\kappa \Delta T_s/q"H))^{2/5} \qquad \textit{(Eq. 10)}$$

where κ is the thermal conductivity of the fluid and q" is the imposed heat flux.

We next redefine the stratification parameter, S, for the uniform heat flux case as,

$$S \equiv \kappa \Delta T_s/q"H \qquad \textit{(Eq. 11)}$$

Notice that S can be interpreted here as the ratio of the vertical heat conduction rate in the fluid to the heat input rate at the wall. This definition was also used by Uotani [11]. Upon inspection of Eqs. (10) and (11), we can define a "stratified" Nusselt number as reflected in the following final equation. He we introduce the notation, "sNu", to represent the Nusselt number in stratified natural convection. For natural convection in liquid metals, we thus have,

$$sNu_x \equiv Nu_x/(1+\lambda Nu_x S)^{2/5} \sim Bo_x^{*1/5} \qquad \textit{(Eq. 12)}$$

We note here that the stratification parameter appears as part of a factor thaty modifies the non-stratified Nusselt number. The relationship reduces to the non-stratified case when there is no stratification (S = 0). [Do not mistake sNu_x for $Nu_x S$] Following the same procedure, we can also develop the stratified heat transfer relationship for uniform wall temperature at the wall. These equivalent results for both liquid metals and ordinary fluids (Pr > 1) are listed below.

For unifrom wall temperature and low Prandtl number,

$$sNu_x \equiv Nu_x/(1+\lambda S)^{1/2} \sim Bo_x^{1/4} \qquad \textit{(Eq. 13)}$$

For uniform wall temperature and ordinary fluids,

$$sNu_x \equiv Nu_x/(1+\lambda S)^{1/2} \sim Ra_x^{1/4} \qquad (Eq.\ 14)$$

And for constant heat flux and ordinary fluids,

$$sNu_x \equiv Nu_x/(1+\lambda Nu_x S)^{2/5} \sim Ra_x^{*1/5} \qquad (Eq.\ 15)$$

II.4 Application

The validity of the simple analysis resulting in Eqs. (12)-(15) was tested with the data of Uotani [10] and that of the first author's [11]. Their heat transfer results presented in the traditional manner are shown respectively in **Figures 2** and **3.** Uotani conducted a natural convection experiment with a vertical plate held at constant heat flux immersed in a bath of lead-bismuth eutectic (Pr ~ 0.025). He showed that due to a reduction in the boundary layer thickness with stratification (steeper temperature gradient), the heat transfer coefficient was enhanced four to five times the non-stratified case for various S-values defined by Eq. 11. At the same time, he verified that the laminar correlation of Chang and Akins [12] was valid up to $\mathbf{Bo_x^* \sim 6 \times 10^8}$. In the first author's case, a natural convection experiment was conducted in a vertical, quasi-rectangular enclosure with one wall held at constant heat flux and the opposite wall water-cooled. (the tapered part of the enclosure was for magnetohydrodynamic studies) The heat transfer medium was mercury. The heat transfer data showed the "shifted" trend for five different heat fluxes, partially as a result of increasing stratification which is evidenced by the bulk temperature profile in **Figure 4 .** (the other major contribution is that due to the aspect ratio of the enclosure; see Ref. 11). The data at low heat fluxes agreed with the laminar correlation and showed a smooth transition to the "1/3rd" slope characteristic of turbulent natural convection at $\mathbf{Bo_x^* \sim 6 \times 10^6}$.

Unfortunately, after surveying the literature, while there are a fair number of investigations on the influence of stratification in natural convection, we have not been able to find additional examples whereby the stratification was quantified and incorporated in some manner into the heat transfer results. There were a few studies in gases (air), but since gases have a very large Prandtl number relative to liquid metals, the influence of stratification are not as apparent when presented in terms of theheat transfer. Besides, experimental results from natural convection in the past 50 years exhibit up to 30% scatter as summarized by Gebhart et al. [3].

When we recast Uotani's data in terms of the stratified Nusselt number versus the Boussinesq number we get **Figure 5** with a linear regression line as given. In this case, the free parameter λ was assigned a value of one since *apriori* we expect ΔT_s and ΔT_w to be of similar magnitude (*not necessarily the same*), and do not expect, for instance, one to be 10 times the other based on some physical argument. One can clearly see that the datum points have collapsed along the calculated regression. In the latter case, a recasting of the data also produced a collapse along a calculated linear regression line (**Figure 6**) . The S-parameter values are noted in the legend. The data from these experiments therefore seem to support the validity of our analysis. We thus expect Eqs. (13)-(15) to be verified in a similar manner.

Having demonstrated the usefulness of OMA in *fine tuning* accepted dimensionless groups that are derived from idealized configurations, we next present another type of flow where in the data analysis phase, we found use for OMA. The study was an experimental investigation on penetrating flow under mixed convection. An introduction is first given, followed by a description of the experiment, results from measurements and finally, the use of OMA in the penetration depth correlation.

III. Penetrating flow under mixed convection

Within the realm of system functions of the Liquid Metal Fast Breeder Reactors, the inherent and passive safety features are of paramount importance. One such feature should provide adequate and reliable removal of decay heat by natural circulation. In particular, the Direct Reactor Auxiliary Cooling System (DRACS) is one of the primary decay-heat removal systems in FBRs. During the operation of the DRACS, relatively cold temperature coolant from the heat exchangers, directly immersed within the hot plenum, are thought to flow down to and into the subassemblies under certain natural circulation conditions. Such phenomenon have already been observed in water-based experiments Hoffmann [13], Ieda [14], Kobayashi [15] and similar phenomenon may occur for example in pressurized thermal shock (PTS) of a pressurized water reactor (PWR) Iyer and Theofanous [16]. In LMFBRs however, the enhanced thermal diffusivity (relative to water) of the coolant, which is typically sodium, amplifies the thermal impact on structural materials as well as influencing the natural circulation head which determines the core flow rate and thus, the core coolability. It's thus evident that a basic understanding of buoyancy-driven flow penetration from both a system design and operational viewpoint, as well as from safety considerations is needed. Since the source of the flow is buoyancy-driven, but within a forced convective environment, it bears noting that these are mixed convective flows.

As for past investigations on mixed convective penetration flows, studies have been conducted the following: Barakat and Todreas [17], Todreas and Luangdilok [18], Todreas and Jerng [19] and Jerng and

Todrreas [20]. While Barakat and Todreas studied backflow or penetration flow from a cooled, upper volume (plenum) into an annulus defined by a concentrically positioned and heated, and an unheated outer cylinder, Jerng and Todreas investigated flow through a heated rod-bundle section enclosed by various means (various shrouds) and also connected at the top to a cooled, upper plenum. In Barakat's work, the authors identified two cases of penetrating flow, mainly: 1) at relatively low to medium heat input where the backflow penetration depth increases with heat input and is controlled by a balance of buoyancy and shear/inertial forces and 2) at higher heat input and higher flow rates through the annulus, where penetration depth remains constant or decreases due to "agitation" inherent in the flow. Barakat and Todreas presented their data, for example the penetration depth in terms of the dimensionless ratio, Gr_q/Re or $Gr'_{\Delta T}/Re$, where the Grashof number is based on respectively, either the heat flux input or the temperature difference between the "cold" penetrating flow and the heated flow. On the other hand, Jerng and Todreas derived the grouping, Gr_T/Re^2, from the conservation equations using a idealized control volume analysis of the exit region where the onset of backflow is assumed to take place at an imaginary plane. The Grashof number in this case is based on the equivalent hydraulic diameter and the temperature difference between the temperature at the exit, T_{out}, and slightly above it at the "onset" plane, T_{on}. Their analysis included use of an assumed axial temperature gradient containing a constant *n*. One of their results showed that for a cylindrical channel, the ratio Gr_T/Re^2 is constant while for annular regions, this ratio's value depends on the dimensions of the respective channels.

While the above studies were specific to reactor geometry, the more fundamental aspect of the role of buoyancy in forced convection flow along vertical surfaces was originally considered by Sparrow and Gregg [21], who used approximate analytical methods and revealed the grouping, Gr/Re^2, as that describing the "strength" of either natural or forced convection. Later Sparrow et al. [22], experimentally demonstrated in a vertical channel only heated from one side that natural convection flow can indeed induce a mass defect under certain conditions such that there is penetration flow or rather, a downward flowing "make-up" flow from above, into the channel. This penetration flow however, did not influence the heat transfer results. Modi and Torrance[23] also investigated inflow of cold air at the exit of a cooling tower/stack-type configuration and noted that the controlling parameter was the Froude number, which is in fact the inverse of Gr/Re^2 ($Fr = \rho U^2 / gL\Delta\rho$).

IV. Experiment

IV.1 Experimental facility

The experimental facility consists of two independent water-loops as shown in **Figure 7a** with one of them, the cooling loop functioning as the name implies. The primary loop, on the other hand is composed of the

test section defined by a vertical inlet channel, an enclosure with a cooled vertical wall (right-hand-side) and a vertical outlet channel. These sections respectively represent in a conventional FBR design: 1) a subassembly channel connected to and 2) a hot plenum with a heat-exchanger (of DRACS). The facility however was not intended to be a scaled-down FBR, but rather a simple apparatus in which the penetration flow could be isolated and investigated. The figure thus shows the operationally measured flowrates and temperatures, as well as the simple bell-mouth arrangement in the head tank that maintained flow through the test section to within 0.1 l/min. The inlet flow temperature was controlled within the stirred heating tank, while a cryostat controlled the temperature of the cooling loop. Both the cooling and inlet temperatures were maintained within 0.2°C of the desired setpoint. **Figure 7b** shows an enlarged view of the test section. The "plenum" enclosure is 150 mm in width and is made from acrylic resin so that it is transparent for flow visualization and LDA. The working fluid was water. Heated water enters the inlet channel 1500mm in length through a flow straightening section situated at the bottom. The cooled-wall at the right edge of the enclosure consists of a copper plate heat exchanger with a 5 mm thick wall (facing the test medium) and a serpentine internal flow-channel pattern inside a "cooling box" with the inlet/outlet pipes at bottom/top respectively. The coordinate system is also shown in **Figure 7b**.

As for measurement methods and probes, temperature measurements were taken with 1 mm diameter, T-type (copper-constantant) thermocouple (T/C). There were two types of configurations: 1) fixed probes arrays and 2) traversing arrays. The locations of the fixed array of T/Cs are shown as dots in **Figure 7b** while the traversing array, which was inserted into the inlet channel, consists of 5 TCs on an horizontal T-branch. Four of the five TCs are placed closer to the right-hand side (the "cold flow" side) of the channel.

Velocity measurement in the plenum and in the inlet channel were initially made by a two-dimensional LDA-system with a computer-controlled *x-y-z* traversing mechanism. The laser was a Coherent 5W argon gas laser. Per given position, the average of 500 sampled points were used as the measured result. This required 5 to 20 minutes per position. At a later stage, additional velocity measurements were made by Ultrasonic Velocity Profile (UVP) monitor which operates on the principle of pulsed ultrasound (Doppler) echography. The UVP can measure a velocity profile along a ultrasound beam line in a vector form; that is, the UVP detects flow toward and away from the front face of its transducer at 128 locations along it's beam line, thereby producing a bi-directional distribution. Flow-tracing powder added to the loop act as ultrasound reflectant in the flow. In the experiment we used Expancel powder with a density, 1.02 gm/cm^3, and nominal particle size, 50 μm. A fresh velocity profile is produced on a computer monitor every ~300 msec along 128 points. The ultrasound transducer was directly immersed in the plenum and although its orientation was adjustable, it faced vertically downward, approximately 2 mm above the right-hand wall of the inlet channel. **Figure 7b** shows an enlarged view of the UVP transducer location in our experiment and the line of measurement (of the ultrasound beam), which we designate as *LM*.

IV.2 Experimental test cases

A number of different types of experiments were carried out with the described test facility over a rather long period of time. The experimental parameters were: 1) the inlet temperature of the vertical channel, 2) the temperature of the feedwater at the cooling box and 3) the inlet velocity of the channel based on the measured flowrate with a hydraulic diameter of the channel (D_e=0.075m). With these parameters, the experimental cases are as those indicated in **Table 1**. The purpose and measurement method(s) associated with Table 1 and the corresponding stages of the experiment can be briefly summarized as follows.

Experiment I. LDA velocity measurements were made in the plenum in order to understand the flow patterns within the plenum.

Experiment II. Simultaneous UVP and T/C measurements were carried out inside the channel. The purpose was to obtain at least a qualitative understanding of the correlation between the penetration flow and temperature distribution. Four cases marked A, B, C and D in Table 1 describe the experimental conditions. The inlet velocity was varied as the test parameter. The data sampling time for velocity and temperature measurement were 137 seconds, and the sampling interval was 0.13 seconds.

Experiment III. Temperature measurements were carried out by a traversing T/C set inside the channel inlet. All the cases indicated (lettered) in Table 1 were covered. The purpose was to gather enough data so that a correlation describing the onset condition of penetration flow and penetration depth could be produced. Thirty test cases were carried out. The data sampling time was 10,000 seconds (about 2.78 hours) and the sampling interval was 0.5 seconds.

V. Results

V.1 LDA velocity plots

In order to first provide the reader with an idea of the flow field within the test section, a representative LDA-produced velocity vector plot is shown in **Figure 8**. In Fig. 2, the inlet temperature was 48.9°C and the cold wall temperature was 14.8°C. The inlet velocity was 4.1 cm/s. It is easy to see several distinct features of the flow field; that is, besides the forced flow from the inlet channel up the left-hand wall and along the "roof" (slanted top surface), there are two counter-rotating vortices with the one near the cooled-wall, oriented clockwise. The velocity vectors outlining the counter-clockwise-rotating vortex is smaller in

magnitude than the other and perhaps difficult to see. Based on the reference vector shown in the figure, the forced flow near the roof appears to be an order of magnitude larger than the flow along the bottom wall. The negatively buoyant flow from the cooled wall also appears to impinge the bottom wall and subsequently, induces a vertical velocity component near the corner region before becoming largely horizontal. An increase in the average inlet velocity to 11.4 cm/s, a slight change in inlet temperature to 49.1°C and cold wall temperature to 15.4°C did not change the overall features of the flow pattern; that is, although the flow velocity along the left-hand wall and roof was enlarged by a factor of 2, the horizontal flow velocity along the bottom wall, toward the inlet channel, maintained its value at approximately 1cm/sec.

V.2 Velocity and temperature profiles

The results of the LDA measurements can be further verified by a representative set of velocity (LDA) and temperature profiles along a vertical traverse shown in **Figure 7a** (also **Figure 8**). The data shown are along line A-A in Fig. 2. The plot shown correponds to test conditions given in **Figure 8**. It is evident from the velocity profile that near the bottom (z-axis), the flow is of order O(~1 cm/s) for $0 < z < 50$ mm and decreases to 0 cm/s at approximately $z \sim 150$ mm. Subsequently for $150 < z < 200$ mm, there is no x-component, V_x, of flow. Thereafter, between $200 < z < 450$ mm, there is flow toward the left-hand wall that is a part of the counter-clockwise rotating vortex shown in **Figure 8**. This also suggests that there is a *thin* region of high shear where the upward forced flow meets the z-component of this counter-clockwise circulationg vortex. Finally, for $z > 450$ mm, there is a sharp increase in V_x up to 6 cm/s, along the upper reaches of the slanted wall.

The corresponding average temperature profile taken along the same traverse as the velocity shows an overall ($0 < z < 550$ mm) temperature stratification ~9°C, but most of this is established over the first $0 < z < 250$ mm, as the temperature is quasi-constant for $z > 250$ mm. This also means that in the aforementioned region of high shear, there is interestingly no apparent temperature gradient. The nearly flow *stagnant* region however ($150 < z < 200$ mm), is thermally stratified. It is also worth noting that within the horizontally flowing liquid at the bottom of the test section, the temperature increase is approximately 4°C (39° to 43°C) over its 50 mm *thickness*. This means that there is temperature gradient within the creeping "cold" flow. The inlet temperature for this case was 48.9°C.

The actual temperature signal for those cases in which there is flow penetration is next shown in **Figure 11** as a sequence of four, at various depth into the channel with each showing a 140 second time-span. One can clearly see that, owing to the dynamic thermohydraulic balance at the *hot-cold* interface, the recorded

temperature signal at a particular z-depth fluctuates 6-8°C in a matter of few seconds. In particular, when there is flow penetration there is a temperature decrease as also observed by Barakat and Todreas [17]. In addition, the figure indicates that there are fewer fluctuations at deeper depths; that is, while penetration of cold fluid to z~10 mm was common, penetration to z~40 mm based on temperature data alone appears less frequently.

V.3 UVP measurements

A limited amount of velocity data has been taken using a device called the Ultrasound Velocity Profile monitor manufactured by **Met-Flow SA.** The device which operates on the principle of ultrasound Doppler echography has been most notably used and described by Takeda [24,25,26] in a number of applications. In **Figure 11a** and **b** we depict a typical spatio-temporal plot, color-coded in magnitude, of both the UVP measured velocity and thermocouple-derived temperature. Both plots show a 137 second time-period along the same measurement span, -10 to -70 mm into the channel. The largely *green-blue-purple* shades represent the penetration flow into the channel, reaching in the case shown a maximum penetration depth of ~70 mm and a maximum *free-fall* velocity of 70 mm/s. The corresponding upward velocity is 30 mm/s at a distance 1mm from the wall. In **Figure 11b** one sees an expectedly similar color-coded temperature pattern as in **Figure 11a** since the penetrating flow transports in a sense, lower temperature fluid into the higher temperature forced flow. While a quantitative correlation between velocity and temperature signals was not made, we nevertheless heeded the qualitative similarity in **Figure 11** and subsequently based our investigation of the penetration depth on the pointwise measured temperature data like those shown in Figure 4.

VI. Discussion of Results

VI.1 Penetration depth correlation

Temperature data was thus taken at 10 depth-locations inside the channel and for each, instances of temperature decrease were counted over a 10,000 second (2.78 hours) period. We called this the penetration frequency. The 10,000 second span was arbitrarily chosen as a sufficiently long time-span for measurement and the *maximum* penetration depth was further defines as the depth at which the penetration frequency fell below 10 counts over 10,000 seconds. Successive temperature decreases at two consecutive sampling instances were not counted as two events. We could not discern nor discriminate however, what we observed in our flow visualization experiments as far as penetration phenomena; that is, the thermocouple, fixed at mid-width of the test section, recorded *any* penetrating flow (a temperature drop)

approaching from *all* directions and did not detect single out those from above. Thus penetrating flow crossing this mid-width thermocouple from the side was equally recorded as a penetration event. The result of this simple criterion nevertheless yielded **Figure 12**, whose data points show a definite trend. For the points shown, under set inlet velocity, inlet temperature and cooling box temperature conditions, we evaluated both the Grashof and Reynolds numbers corresponding to the maximum penetration depth. The thermophysical properties of the forced flow were evaluated at the inlet temperature, 1000mm from the exit of the vertical channel, while for the Grashof number, the temperature at the bottom of line A-A (see Fig. 1a) was used as a reference. We then plotted in **Figure 13** the Grashof versus the Reynolds numbers, including data taken from barakat and Toddreas and a limited number of points from a similar experiment conducted in sodium Hayashi et al. [27]. This figure in brief represents regimes, to the right of the regression line where there is no penetrating flow and to the left where there is penetration. The data of Barakat and Todreas were for an annular geometry whose inner boundary itself was the heated surface in contrast to the present experiment. The annular region of flow was connected at the top to a plenum with a cooling heat-exchanger. As mentioned the grouping, Gr/Re^2, is constant for an annulus, as derived from their analysis, and the various constants are noted in the figure. It's also of interest to note that in Sparrow and Gregg [21], the *overall drag* in terms of a ratio of the shear stress at the plate to that due purely to forced convection, for an calculated accuracy of 5%, is also a constant value; that is, the grouping, Gr/Re^2, takes on a value of 0.5175 for Pr=1.0. This is similar to our value.

VI.2 Penetration Depth Correlations and OMA

From an designer's point of view and that concerning thermal stress analysis (i.e. thermal striping), it is desireable to quantify the penetration depth, z/D_e, as a function of dimensionless groups, Gr and Re, which respectively decribe the natural and forced convection. In addition as noted, the grouping, Gr/Re^2, which is also known as the Richardson number, Ri (thus $Ri = Gr/Re^2$), appears in the literature as a measure of mixed convection's inclination toward forced or natural convection. **Figure 14** shows the maximum penetration depth as a function of the Ri-number in the present experiment. In the figure, the correlation equation and the calculated, relatively low value of the correlation coefficient for the regression curve is given. (the data of Barakat and Todreas is discussed with the analysis below.) Since the apparent scatter can be attributed to either: 1) systematic and/or random error from our experiment or 2) the inappropriateness of the Ri-number as the characteric dimensionless number, we first pursued the latter by performing a simple dimensional analysis (Buckingham's π-Theorem). However, first recall that proper scaling of a physical phenomenom should typically be indicated by *collapse* of datum points along a calculated correlation curve along with axes scales of the order, $O(1)$ [1]. When we subsequently model only the buoyancy and inertial forces, thus explicitly neglecting *interfacial* (between hot and cold)

dynamics including convective heat transfer effects, we take as parameters: g, U, β, ΔT, μ, κ, ρ, C_p and two length scales, z and D_e. Note that the heat capacity, thermal conductivity and dynamic viscosity are implicitly included while a *generic* density (since an algebraic analysis precludes any distinction between $\Delta\rho$ and ρ) is adopted. This simple analysis revealed (only) that the penetration depth should be a function of three dimensionless groups, $(z/D_e) = f(Gr/Re^3, Re, Pr)$ and obviously contains the grouping, Gr/Re^2 [$= (Gr/Re^3)*Re$], since the *actual functional form* is determined by experimental data [28]. Therefore using Gr/Re^2 appears valid, but equally, additional possibilities also exist such as Ra/Re^2 [$=(Gr/Re^3)*Re*Pr$] or even Gr/Re^4 [$=(Gr/Re^3)/Re$]. When we replot **Fig. 14** versus the grouping Gr/Re^3 in **Figure 15**, indeed a correlation with a higher correlation coefficient to that in the figure is obtained. However, it is by accepted tradition in the heat transfer community that mere experimental correlations, though valid and of value, do not specifically contribute to the understanding of the physical phenomena. In this regard, a physical interpretation of Gr/Re^3 or Ra/Re^2 or Gr/Re^4 based on force or energy balance arguments are neither obvious or forthcoming.

On the other hand, a physical interpretion for Gr/Re^2 does exist and this is simply the ratio of buoyancy to inertial forces. At this point, in order to clarify not only the appropriate dimensionless grouping characterizing this phenomena, since Barakat and Todreas also use, Gr/Re, a further order of magnitude analysis (or scale analysis) was conducted. Once again the inertial force associated with the average inlet flow velocity and the buoyancy-driven cold fluid flow were considered. The results are more general in that both low, ordinary and high Prandtl number fluids are included and in that a functional form containing the dimensionless groups is given.

If we begin with our channel geometry as in **Figure 7b** defined by a channel of length L, equivalent hydraulic diameter D_e, and note the momentum and thermal boundary layers, δ_M and δ_T, respectively representing the forced convection flow from below and the penetrating natural convection-driven flow from above, we know the following.

The momentum boundary layer describing the forced flow in the vertical channel from below is described by,

$$\delta_M/L \sim 1/Re_L^{1/2} = 1/(UL/\nu)^{1/2} \qquad (Eq.\ 16)$$

while the thermal boundary layer describing the flow of the buoyancy-driven cold flow is, firstly for $Pr \ll 1$,

$$\delta_T \sim z(Gr_z Pr^2)^{-1/4} = z[(g\beta\Delta Tz^3/\nu^2)(\nu^2/\alpha^2)]^{-1/4} \quad (Eq.\ 17)$$

These results are available in standard texts such as **Bejan [1]**. The variables are defined in the usual manner.

The corresponding velocity scales are as follows, first for forced convection,

$$U_\infty \sim \alpha L/\delta_T^2 \quad (Eq.\ 18)$$

and for natural convection,

$$v \sim (\alpha/z)(Gr_z Pr^2)^{1/2} \sim (\alpha/z)[(g\beta\Delta Tz^3/\nu^2)(\nu^2/\alpha^2)]^{1/2} \quad (Eq.\ 19)$$

Note here that for liquid metals, meaning Pr <<1, we know tha t since $\delta_M << \delta_T$, the vertical velocity scale (in the channel), u, is in fact $u \sim U_\infty$.

If we assume that *locally* that the penetration depth is only determined by a (force) balance of inertial and buoyancy forces, the force balance is simply described by,

$$U_\infty^2/L \sim v^2/z \quad (Eq.\ 20)$$

Here, as mentioned, we neglect any interfacial dynamics (entrainment, interfacial waviness) and heat transfer effects (conduction and convection) since we are using the simplest model possible. If our analysis is in error, then a comparison of our simple model against experimental data should reveal a discrepancy. If on the other hand, the correlation coefficient or "fit" is good, then we know that our assumptions are essentially correct.

When we substitute Eqs. 18 and 19 into 20 and further note that,

$$(\delta_T/L) \sim Pr^{-1/2} Re_L^{-1/2} \quad (Eq.\ 21)$$

We can then easily solve for the dimensionless penetration depth into the channel, *(z/L)*, and arrive at,

$$(z/L) \sim (Gr_z/Re_L^2)^{1/3} \sim Ri^{1/3} \quad (Eq.\ 22)$$

where we note that (Gr_z/Re_L^2) is the so-called Richardson number.

If we instead want to know the penetration depth normalized by the hydraulic diameter then,

$$(z/D_e) \sim (Gr_z/Re_L^2)^{1/3}(L/D_e)^{1/3} \quad (Eq.\ 23)$$

which reveals the aspect ratio's role in the penetration depth. These are the relations for *low* Prandtl number fluids.

For ordinary fluids such as water and oils, Pr ≥ 1, we again have equation Eq. 18 again but Eq. 19 changes so that,

$$v \sim (\alpha/z)\,(Gr_z\,Pr^2)^{1/2} \sim (\alpha/z)\,[(g\beta\Delta T z^3/\nu^2)(\nu^2/\alpha^2)]^{1/2} \quad (Eq.\ 24)$$

and

$$u \sim (\delta_T/\delta_M)U_\infty \quad (Eq.\ 25)$$

where

$$\delta_T/L \sim Pr^{-1/3}\,Re_L^{-1/2} \text{ and } \delta_M/L \sim Re_L^{-1/2} \quad (Eq.\ 26)$$

The force balance (same as equation Eq. 20) this time reveals,

$$(z/L) \sim (Gr_z/Re_L^2)^{1/3}\,Pr^{2/3} \sim Ri^{1/3}\,Pr^{2/3} \quad (Eq.\ 27)$$

$$(z/D_e) \sim (Gr_z/Re_L^2)^{1/3}(L/D_e)^{1/3}\,Pr^{2/9} \quad (Eq.\ 28)$$

These are the results for Pr ≥ 1. Note here, that in contrast to Eqs. 23 and 25, Eqs. 27 and 28 contain the Prandtl number. This seems to make sense since low Prandtl number fluids usually have values 0.1 to 0.01; that is, they only change an order of magnitude $(10)^{2/9} \sim 1.7$. This means that a 10-fold change in the Prandtl number brings about a 70% change in the penetration depth. In the case of sodium however, since Pr ~ 0.003 there is a two-order change that corresponds to $(100)^{2/9} = 2.78$ (278%). Ordinary fluids however, can change 3 to 4 orders of magnitude from 1 to 10,000 in which case $(10{,}000)^{2/9} \sim 7.74$ (774%) and $(1000)^{2/9} \sim 4.64$ (464%). This appears to support the view that the Prandtl number has a much stronger

influence on ordinary fluids and thus in eqs. 27 and 28, it is included as a dependent parameter. Relations 27 and 28 should also be valid for gases such as air.

Thus if these relationships are correct, Eq. 28 should in the present case (for water) reveal a collapse of the data points in comparison to **Figure 14**. We first show the data of Barakat and Todreas with our data, (z/D_e) versus the Richardson number in **Figure 15**. Then in Figure 16, (z/D_e) is recast versus the grouping, $(Pr^{2/3}*Gr/Re^2)^{1/3}(L/D_e)^{1/3}$. Not only is the Richardson number, (Gr/Re^2), reconfirmed as the charcteristic dimensionless group, but the dependence on the Prandtl number and aspect ratio confirm physical intuition. For both an annulus and a square-channel, the aspect ratio should influence the flow penetration. The exponent, "1/3", as revealed by the analysis appears to be the key. One slightly surprising result in equation (3), is the lack of Pr-number dependence. This observation is considered in the Appendix.

When we apply these results to the annular data of Barakat and Todreas , we observed nearly the same results in comparing **Figure 14** versus **Figure 15**. Their data point values were extracted from the regression curve drawn through their points for all channels in "Region I"; that is, under conditions, as they report, wherein an increase in the buoyancy to shear force ratio increases the penetration depth and while the fluid *agitation* (in the flow channel) is small relative to the backflow (more so at low heat input). The reference "all channels" indicates a plot showing 3 different sizes of annuli. Additionally for values of the grouping, $(Gr'_{\Delta T}/Re)$, smaller than 3×10^2, datum points were read from a second plot for what they called a small channel (D_e =0.635). It is also worth noting that their correlation equation overpredicts the penetration depth for $(Gr'_{\Delta T}/Re)$ approximately smaller than 10^3. Sixteen representative points are thus shown in **Figure 15** along with our points versus (Gr/Re^2) and then recast versus the grouping, $(Gr/Re^2)^{1/3}(L/D_e)^{1/3}$ in **Figure 16**. Because the temperature at which to evaluate the Prandtl number is unknown from their work, we did not plot the points including the Pr-number. It was taken as unity. An slight difference in ΔT used to calculate a value for the Gr-number does not change our conclusion. One can clearly see in **Figure 16** that the points collapse upon themselves although there is still some recognizable scatter in the MIT data. We attribute this partly to the inaccuracies introduced while estimating coordinates for their datum points.

The overall difference in the two data sets, on the other hand, is likely attributable to the Pr-number (as plotted in **Figure 9**), differences in geometry (square versus annular) and a suttle but important difference in the two experiments; that is, the boundary conditions and thus the thermohydraulics. In Barakat and Todreas' experiment, the physical (positive, aiding) buoyancy source in terms of the heater is contained in the test section, while in our experiment there is no such source. The (forced) flow and temperature

boundary conditions in our experiment are thus determined downstream of the test section. In contrast, although the forced flow is determined downstream of their test section, the heat flux is set within their test section. This has significant impact on the results in that no *mass defect* is created within our test section while a mass defect can be created in theirs. In terms of a physical description of penetrating flow, it is said that the local buoyancy-driven acceleration alters the forced flow's velocity profile to such an extent that mass conservation dictates an inflow of fluid from a larger volume located above. This is the case for buoyancy and inertial forces acting in the same direction. In contrast, the penetrating flow in the present experiment is primarily a *free-fall* of cold liquid into a upward flowing, hotter stream of the same liquid. The cold liquid is negatively buoyancy-driven from the cooled wall. In either case, a conclusion that can be drawn is the importance of the balance between inertial and buoyancy forces.

VII. Conclusions

When conducting analytical and experimental investigations into the thermal-hydraulics of nuclear reactors and other energy-related systems, the validity for example of simulation experiments and separate effect studies is determined by the proper identification of dimensionless group(s) and the reproduction of their relevant magnitudes. Since tradition has dictated many of the accepted dimensionless groups, based on highly idealized geometries and configurations, most real experiments contain some simplications such that the relevant dimensionless groups are easily identified. These groups alone however, may not accurately reflect the nature of the real system; that is, the non-ideal nature of any given experiment may for instance appear in the presentation of data using just the selected groups. If this is the case, a reconsideration of the dimensionless groups via Scale Analysis or Order of Magnitude Analysis (OMA) may reveal slight modifications to classic results that originate from ideal cases. The present work summarizes the use of OMA in such a situation as described; that is, we consider the stratified natural convection problem from which a stratified Nusselt number is introduced. Two data sets are presented in support of the described modification.

After this, we reported on an experimental investigation of buoyancy-driven penetration of cold liquid into a vertical channel, under forced, upward flow of a hotter liquid in the channel. The test medium was water. The vertical channel simulated a subassembly channel connected to an hot plenum of a prototypical FBR design. Besides stationary and traversing temperature measurements, velocity measurements were conducted using LDA and UVP, the latter in particular for investigating the penetrating flow. In the earlier phases of experiments, temperature measurements revealed that the colder water crept along the bottom, horizontal wall of the hot-plenum while the hotter fluid flowed along the upper regions. The plenum itself is nearly a square enclosure except for the top wall which is slanted like a roof. LDA measurements

confirmed these flow patterns and additionally identified a counter-rotating pair of vortices, along which temperature gradients were very small in comparison to the uppermost and lowermost regions. Subsequent comparison of UVP and temperature spatio-temporal measurements revealed an overall likeness in their signatures as expected. With this in mind, temperature measurement alone were used to identify flow penetration of colder fluid into the channel. This was done by measuring the frequency of temperature decreases with respect to hotter flow at various depths in the channel. A criterion for penetration and a subsequent plot describing the onset of flow penetration were developed in terms of dimensionless groupings. The identified dimensionless groups were the Grashof, Reynolds and Richardson numbers, the last of which could be expressed in terms of the first two as, $Ri = Gr/Re^2$. The Ri-number and Gr/Re have been reported in the past as characterizing mixed convection penetrating flow. When we however, plotted the penetration depth as a function of Ri-number, we found unsatisfactory scatter in our data with respect to a regression curve. We thus reconsiderred these dimensionless parameters and after conducting an OMA we deduced that, $(Gr/Re^2)^{1/3}$, was the essential part of the proper functional relationship for this specific experiment. The difference between this and previous studies were pointed out. A comparison with a previous investigation verified our assertion in this regard.

Nomenclature

Bo_{x^*}: Bousssinesq number, ≡ $(g\beta\Delta Tx^3 / \alpha^2)$
Bo_x^* : modified Boussinesq number, (= Nu*Bo), (=Ra*Pr)
D_e: hydraulics diameter of the inlet channel [mm]
Gr_z: Grashof number, ≡ $(g\beta\Delta Tz^3 / \nu^2)$
H : characterisitic heated length
L: length of the inlet channel [mm]
Nu_x : local Nusselt number
O: means "the order of" as noted in (--)
Pr: Prandtl number, ≡ (ν/α)
Ra_x: Rayleigh number, ≡ $(g\beta\Delta Tx^3 /\alpha\nu)$
Ra_x^* : modified Rayleigh number, ≡ $(g \beta q''x^4 / \alpha\nu\kappa)$
Re: Reynolds number of inlet channel, = VD/ν
S: stratification parameter
sNu_x : stratified Nusselt number
T_{bottom} , T_{top} : top and bottom bulk temperature
T_w : wall temperature
$T_{\infty, x}$: local bulk temperature
ΔT: temperature difference, [K]
ΔT_s: stratified temperature difference, ≡ T_{top} - T_{bottom}
ΔT_x: wall to bulk temperature difference, ≡ T_w - $T_{\infty, x}$
x,y z: Cartesian coordinate, axial distance down the channel as measured from the exit plane, [mm]

Greek Symbols

α: thermal diffusivity, [m^2/s]
β: coefficient of thermal expansion, [1/K]
δ : boundary layer thickness [mm]
κ: thermal conductivity, [w/m^2 K]
λ : free parameter
μ: dynamic viscosity, [kg /m s]
ν: kinematic viscosity, [m^2/s]
ρ: density, [kg/m^3]

References

[1] A. Bejan, Convection Heat Transfer, John Wiley and Sons, New York, USA, 1984. pp. 19-20, 142-146.

[2] Y. Jaluria, Natural Convection Heat and Mass Transfer, Pergamon Press, Ocford, UK, 1980.

[3] B. Gebhart, Y. Jaluria, B. U. Sammakia and R. L. Mahajan, Buoyancy Induced Flows and Transport, Hemisphere, New York, USA, 1988.

[4] R. Cheesewright, Natural convection from a plane vertical surface in non-isothermal surroundings, Int. J. Heat Mass Transfer, 10 (1967) 1847-1859.

[5] R. Eichhorn, Natural convection in a thermally stratified fluid, Prog. Heat Mass Transfer, vol.2, T.F. Irvine Jr. et al. eds., Pergamon, Oxford, UK 1969.

[6] K. T. Yang, J. L. Novotny and Y. S. Cheng, Laminar free convection from a nonisothermal plate immersed in a temperature stratified medium, Int. J. Heat Mass Transfer, 15 (1972), 1097-1109.

[7] M. Takeuchi, Y. Ota and Y. Tanaka, Laminar natural convection heat transfer from a flat plate in a thermally stratified fluid, Trans. J.S.M.E., 40 (1974), 1056-1072.

[8] T. Fujii, M. Takeuchi and I. Morioka, Laminar boundary layer of free convection in a temperature stratified environment, 5th Int. Heat Transfer Conf., Tokyo, Japan, 1974, pp. 44-53.

[9] Y. Jaluria and B. Gebhart, Stability and transition of buoyancy-induced flows in a stratified medium, J. Fluid Mech., 66, pt. 3 (1974), 593-612.

[10] M. Uotani, Natural convection heat transfer in thermally stratified liquid metals, J. Nucl. Sci. Technol., 26(6) (1987), 442-451.

[11] A. T. Tokuhiro, Natural convection heat transfer enhancement with gas injection and in the presence of a transverse magnetic field, Ph.D. Thesis, Purdue University, West Lafayette, Indiana, USA, 1991.

[12] B. H. Chang and R. G. Akins, A experimental investigation of natural convection in mercury at low Grashof numbers, Int. J. Heat Mass Transfer, 98 (1972), 512-525.

[13] H. Hoffmann, Y. Ieda, D. Weinberg, K. Marten, H.H. Frey, H. Tschöke and K. Dres, Investigations on decay heat removal by natural convection for LMFBRs, Proc. 4th Int. Top. Mtg. Reactor Thermal Hydraulics (NURETH-4), Karlsruhe, FRG (Germany), October 10-13, 1989. pp. 384-391.

[14] Y. Ieda, K. Hayashi, H. Kajiwara, K. Satoh, Y. Okabe, M. Akutsu, K. Iwashige, Y. Shibata, H. Wada and K. Ogura, Natural circulation decay heat removal for a pool-type LMFBR, Proc. Int. Conf. on Fast Reactor and Related Fuel Cycles, Kyoto, Japan, October 28-November 1, 1991. pp. 16.9-1 to 16.9-10.

[15] J. Kobayashi, H. Ohshima, H. Kamide and Y. Ieda, Penetration flow of coolant into a core from a plenum during natural circulation decay heat removal - fundamental water experiment, Proc. 29th Den-netsu shinpo-jiumu (29th National heat transfer symposium), Paper B153, Osaka Kokusai Kouryu Center, Osaka, Japan, May 1992 (in Japanese). pp. 98-99.

[16] K. Iyer and T.G. Theofanous, Decay of buoyancy-driven stratified layers with application to pressurized thermal shock: reactor predictions, Nucl. Sci. Eng., 108 (1991) 184-197.

[17]A.I. Barakat and N.E. Todreas, Mixed convection buoyancy-induced backflow in a vertical single-rod channel connected to an upper plenum, Proc. 4th Int. Top. Mtg. Reactor Thermal Hydraulics (NURETH-4), Karlsruhe, FRG (Germany), October 10-13, 1989. pp. 746-752.

[18] N. E. Todreas and W. Luangdilok, Flow reversal under mixed convection conditions in rod bundles, Massachusetts Institute of Technology, Department of Nuclear Engineering, Topical Report No. PNC/MIT-DHR-20TR, Cambridge, Massachusetts, USA, June 1990.

[19] N. E. Todreas and D. W. Jerng, Mixed convective flow reversal in a vertical rod bundle channel, Massachusetts Institute of Technology, Department of Nuclear Engineering, Topical Report No. PNC/MIT-DHR-27TR, Cambridge, Massachusetts, USA, February 1992.

[20] D. W. Jerng and Neil E. Todreas, Mixed convective flow penetration in vertical channels, Proc. 5th Int. Top. Mtg. Reactor Thermal Hydraulics (NURETH-5), Salt Lake City, Utah, USA, September 21-24, 1992. pp. 1720-1728.

[21] E. M. Sparrow and J. L. Gregg, Buoyancy effects in forced convection flow on vertical surfaces, J. Applied Mechanics, 26 (1959) 133-134.

[22] E. M. Sparrow, G. M. Chrysler and L. F. Azevedo, Observed flow reversals and measured-predicted Nusselt numbers for natural convection in a one-sided heated vertical channel, Trans. ASME, J. Heat Transf., 106 (1984) 325-333.

[23] V. Modi and K.E. Torrance, Experimental and numerical studies of cold inflow at the exit of buoyant channel flows, Trans. ASME, J. Heat Transf., 109 (1987) 392-399.

[24] Y. Takeda, Velocity profile measurement by ultrasound Doppler shift method, Int. J. Heat Fluid Flow, 7 (1986) 313-318.

[25] Y. Takeda, Velocity profile measurement by ultrasound Doppler shift method, Nat. Heat Transfer Conf., Philadelphia, USA, ASME-HTD 112, 1989. pp. 55-160.

[26] Y. Takeda, Development of an ultrasound velocity profile monitor, Nucl. Eng. Des. 126 (1991) 277-284.

[27] K. Hayashi, K. Komatsuzaki and K. Kamide, Onset condition of fuel assembly penetration flow in sodium, Proc. Atomic Energy Society of Japan, JAERI-Tokai, Japan, October 17-20, Paper E54, 1995. p. 360.

[28] J. Fox and A. MacDonald, Introduction to Fluid Mechanics, John Wiley and Sons, New York, USA, 1980. pp. 285-295.

Acknowledgement

The first author would like to thank PNC for his appointement as PNC International Fellow. This is the first internal publication during his tenure. The authors also acknowledge the initiative of Professor H. Ninokata who originated a number of investigations in penetration mixed convection and the work by Professor Todreas and his co-workers. Gratitiude is also extended to Mr. Itoh and Mr. Onuma of Joyo Sangyo Co., Ltd., who diligently conducted the experimental measurements.

Table 1. Experimental parameters for which data was taken as presented in this work

Temperature at channel inlet, [C]	Temperature of feedwater of cooling box, [C]	Velocity at inlet channel 2.5	[cm/s] 2.75	3	4	5	6	7
50	12.5	A	B	C	D	E	F	G
45	12.5				H	I	J	
40	12.5			K	L	M	N	
35	12.5			O	P	Q	R	
30	12.5			S	T	U		
25	12.5			V	W			
20	12.5			X				
50	16					Y	Z	
50	20					AA	BB	
50	25					CC	DD	

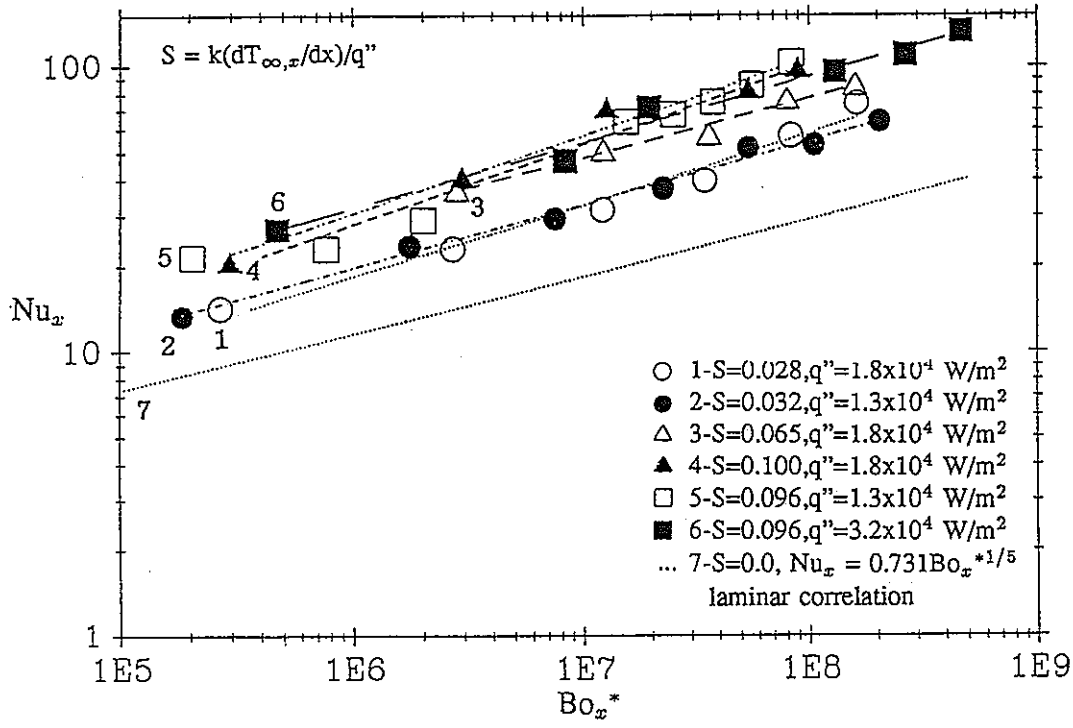

Figure 1. The stratified natural convection data of Uotani.
[Note: Heat fluxes are as noted with the stratification parameter as defined. Laminar correlation is as given]

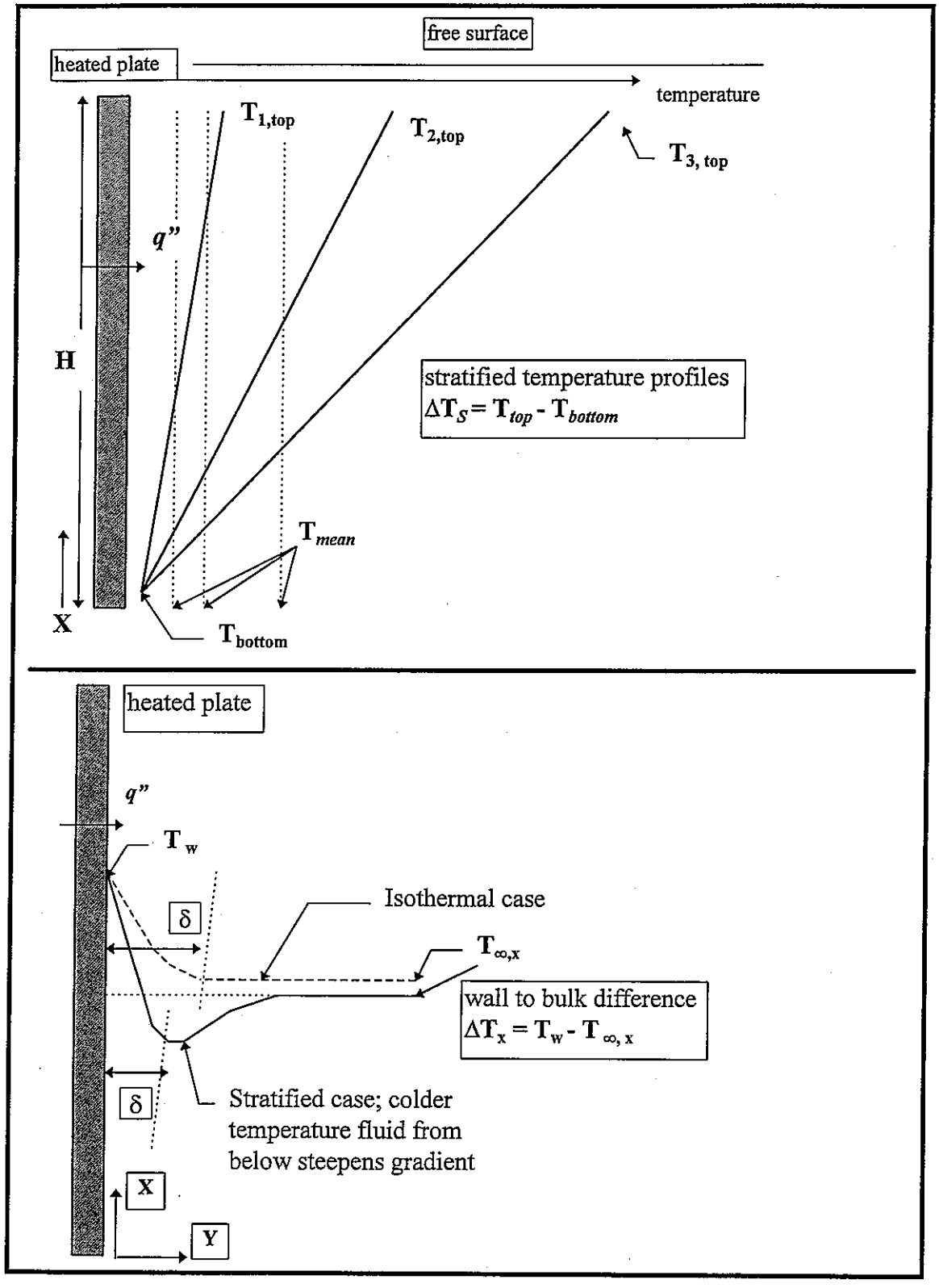

Figure 2. Schematic of a heated vertical plate immersed in a stratified bath.

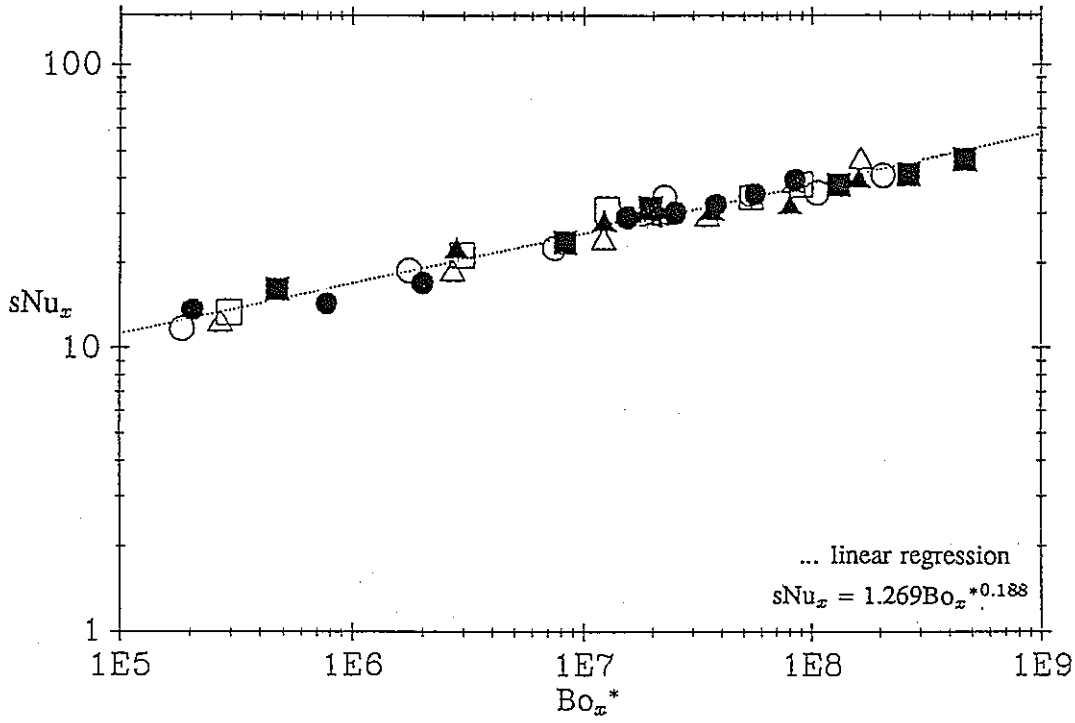

Figure 3. Stratified Nusselt number versus the modified Boussinesq number for the data of Uotani. Recast from Fig. 1.
[Note: Symbols are as in Fig. 1. Correlation is as noted with λ=1.0]

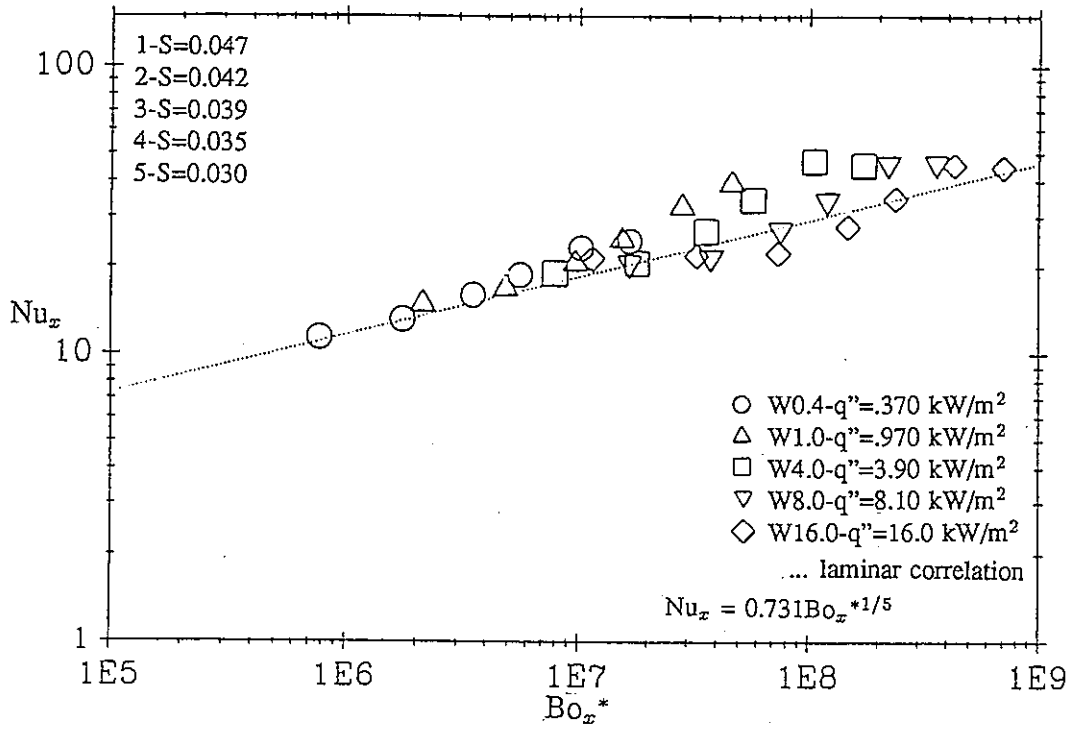

Figure 4. The stratified natural convection data of author.
[Note: Heat fluxes are as noted with laminar correlation. Cf: Tokuhiro]

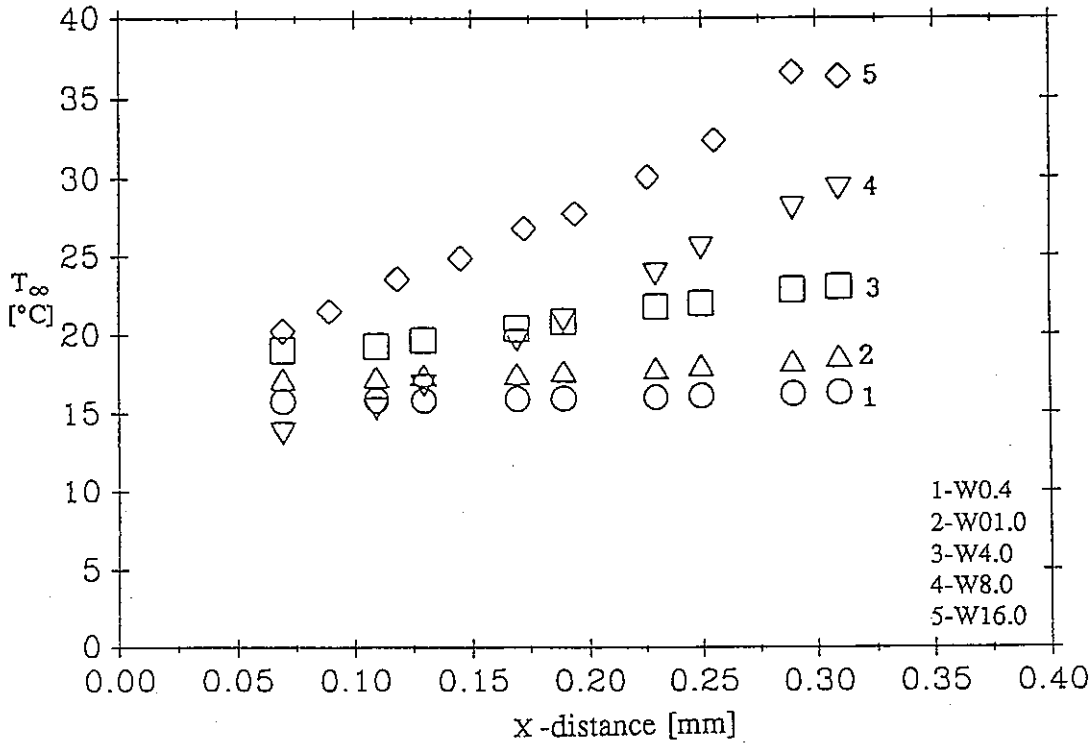

Figure 5. The bulk temperature variation along the heated plate with increasing heat flux (370 W/m^2 < q" < 16,000 W/m^2) [Note: 1=400, 2=1000, 3=4000, 4=8000, 5=16,000 W/m^2]

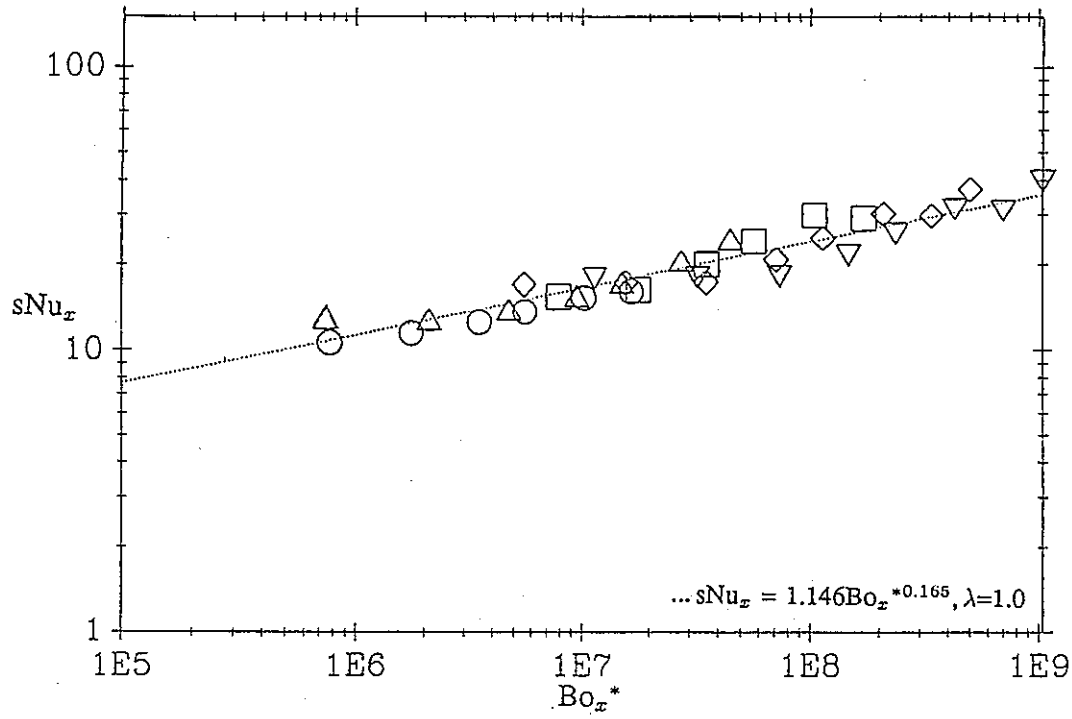

Figure 6. The data presented as the stratified Nusselt number versus the modified Boussinesq number [Note: Symbols are as presented in Fig. 4. Correlation is as shown with λ=1.0]

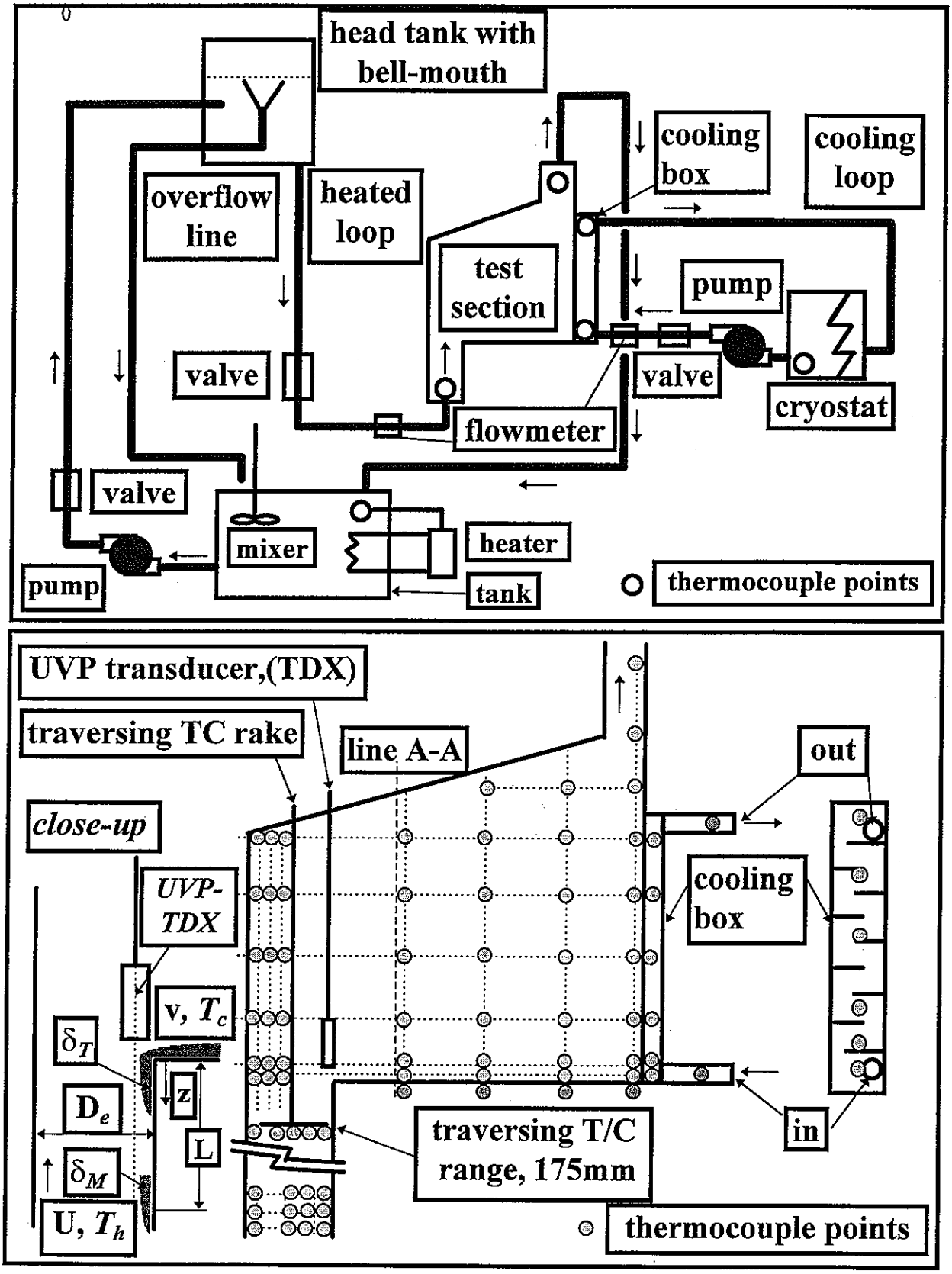

Figure 7. a) Schematic of the experimental loop b) Schematic of the test section with traversing ultrasound probe and thermocouple probe.

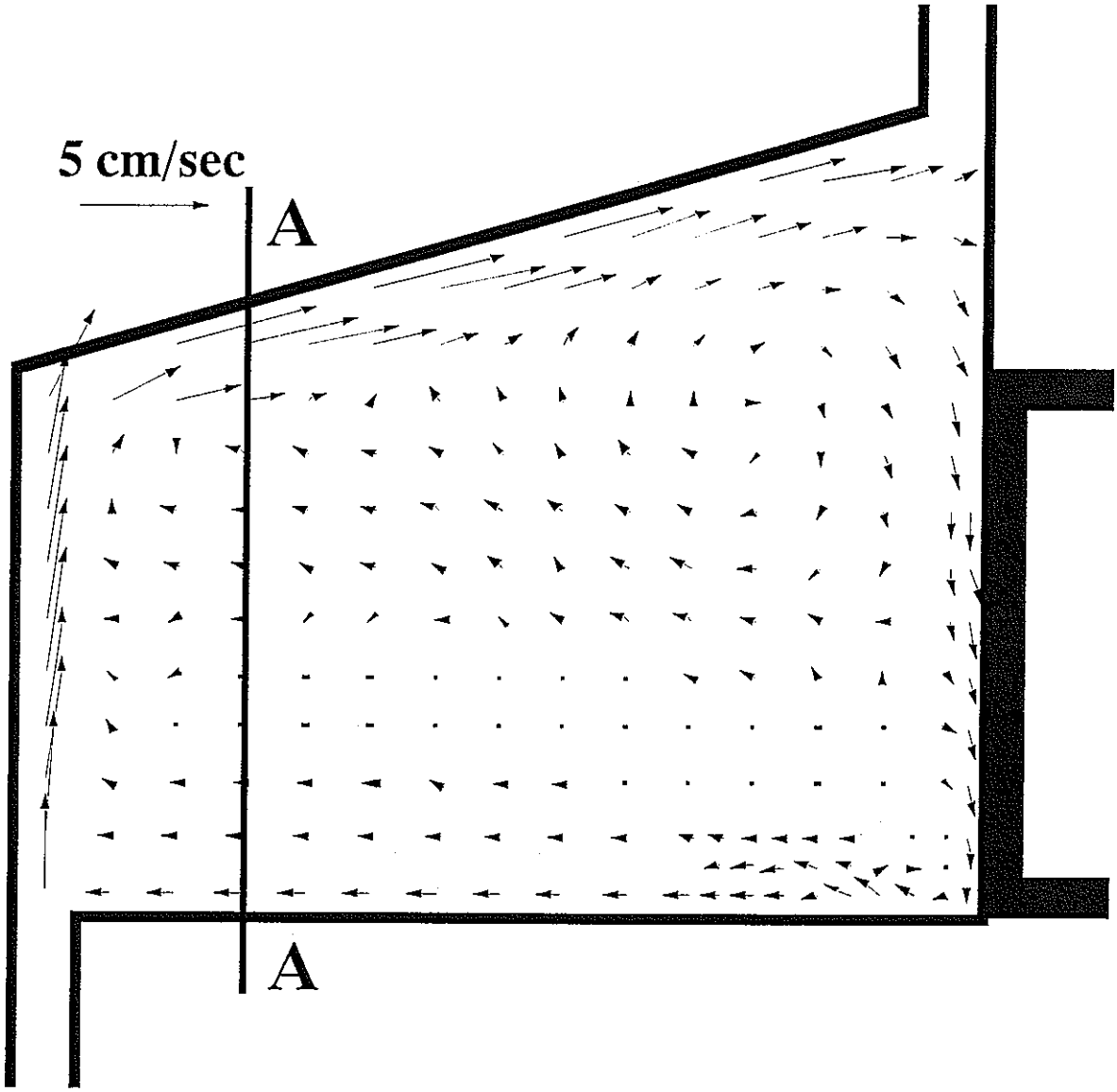

Figure 8. Vector plot of flow within the test section as generated from LDA measurements.

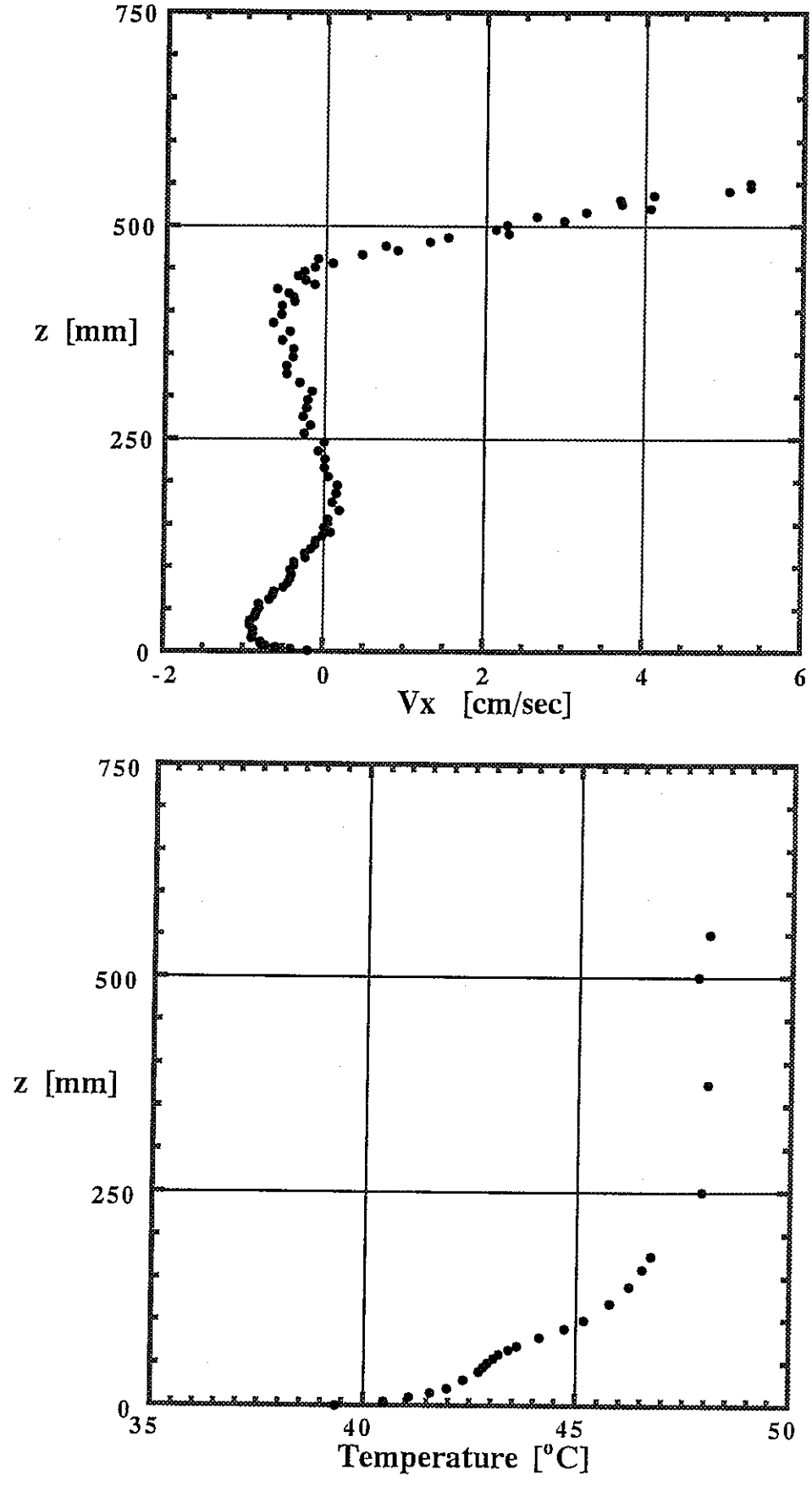

Figure 9 a) Horizontal velocity component distribution along line A-A
b) Temperature distribution along line A-A.

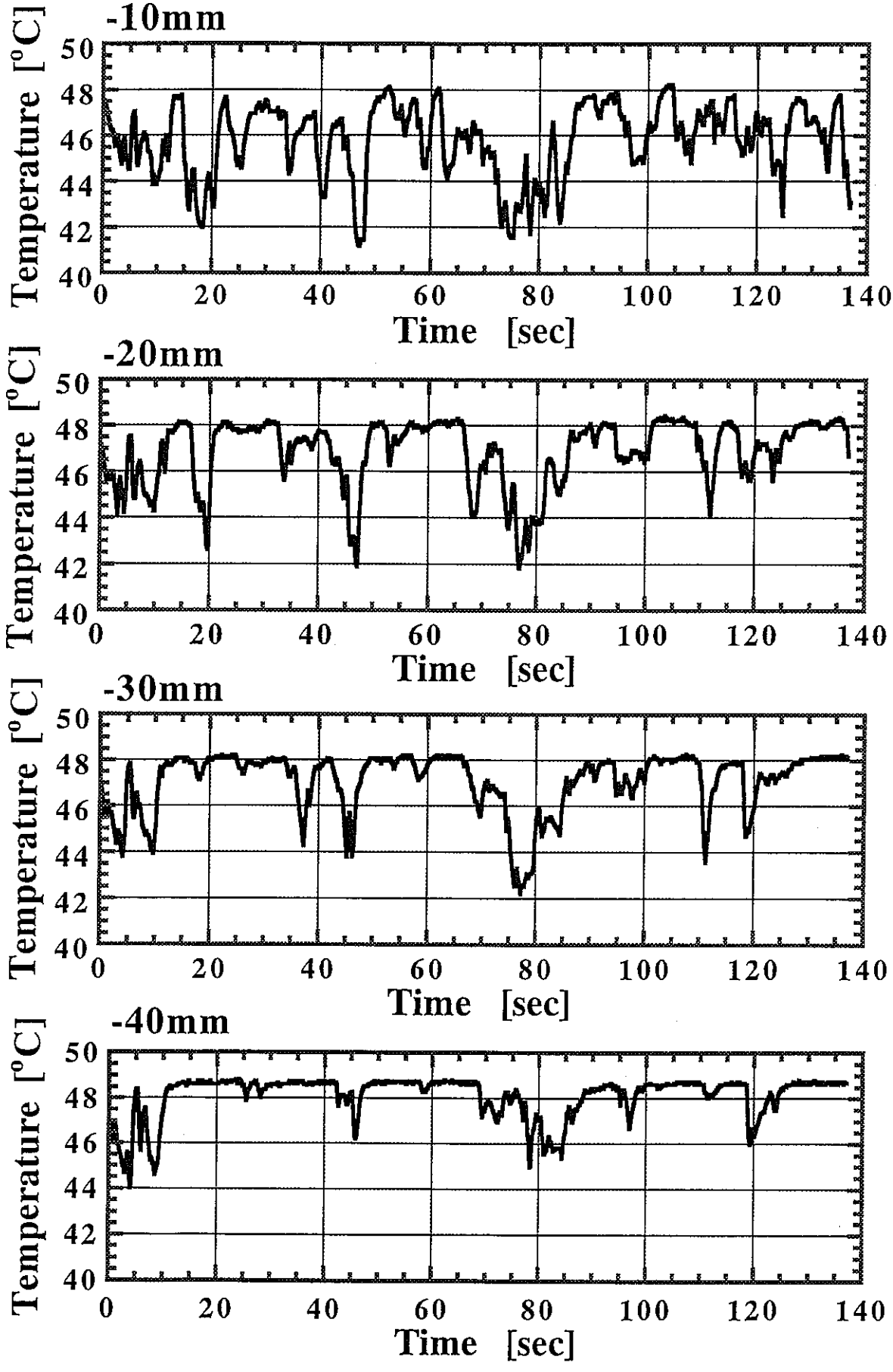

Figure 10. Transient temperature signature of fluid temperature in inlet channel.

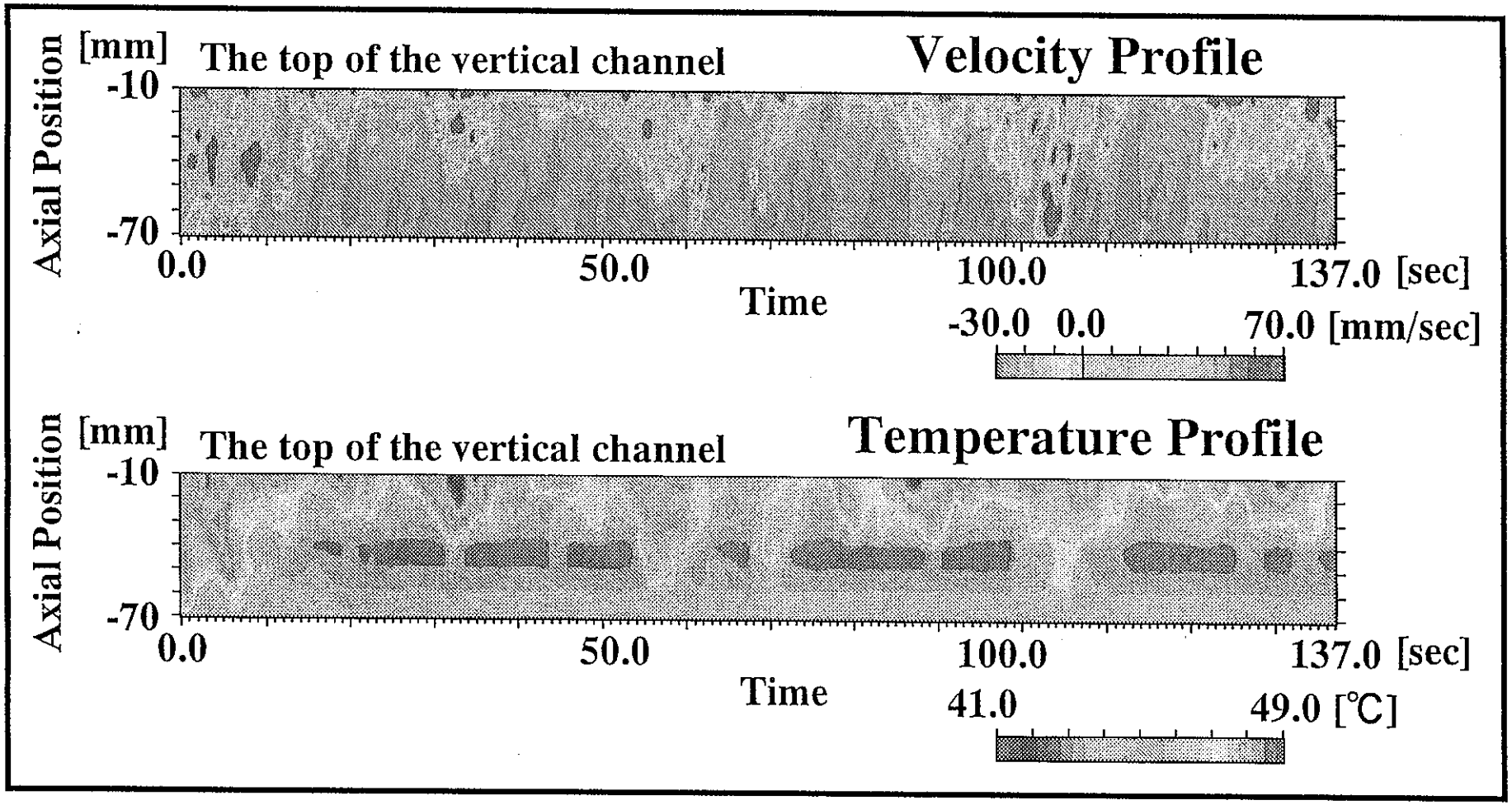

Figure 11. Transient velocity and temperature profiles of penetration flow.

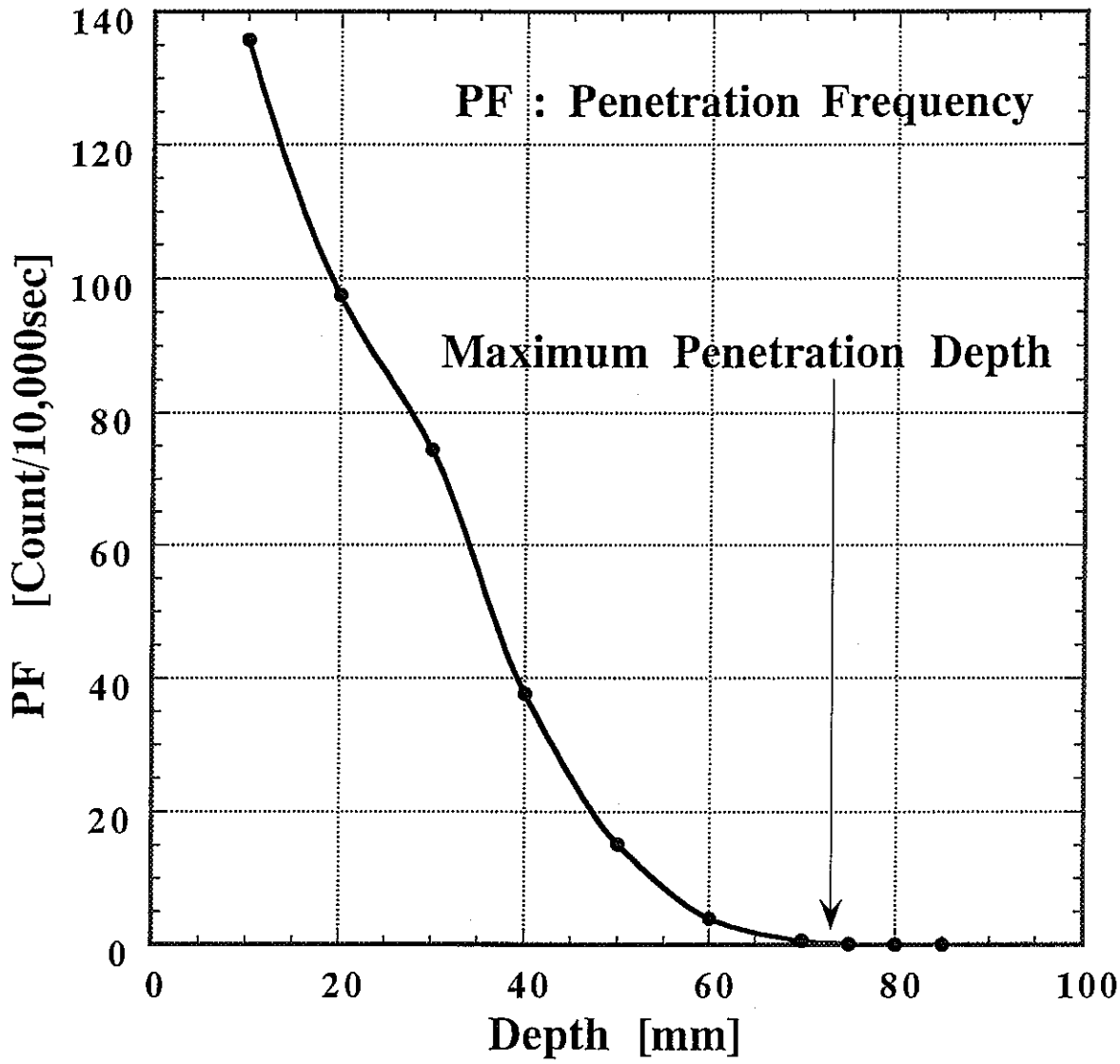

Figure 12. Penetration frequency versus depth into channel.

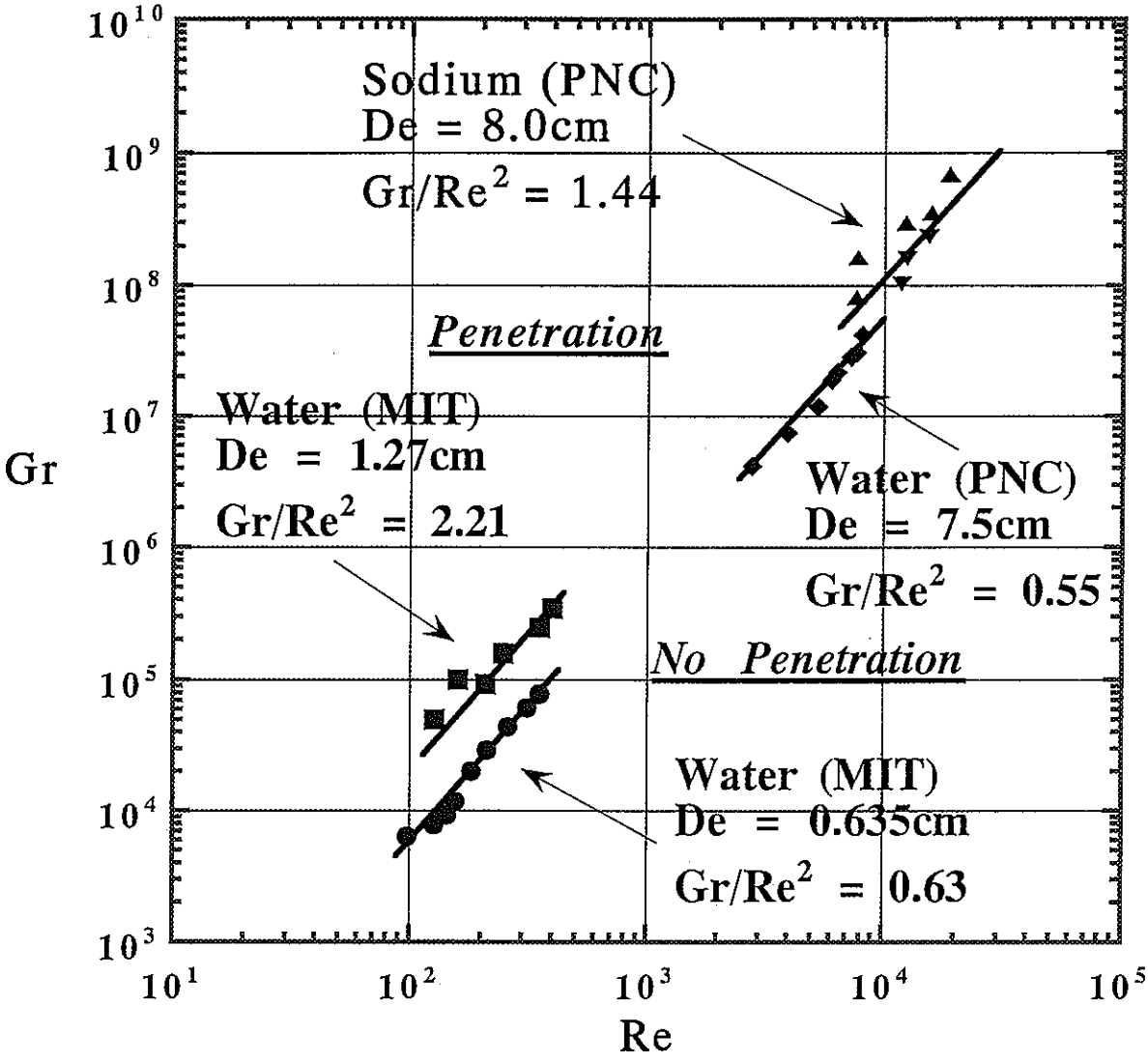

Figure 13. Onset condition for penetrating flow.

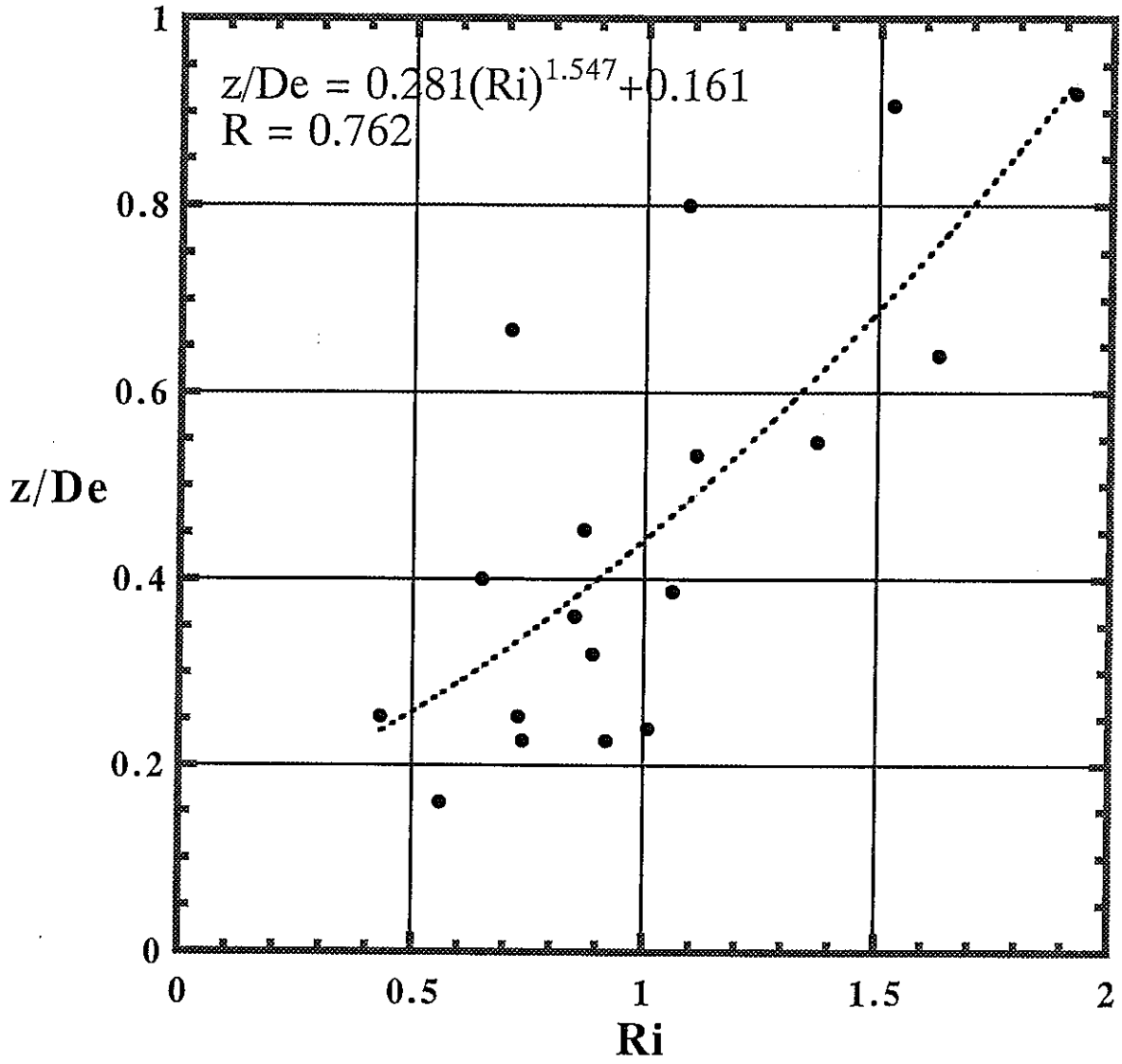

Figure 14. Penetration depth versus Richardson number.

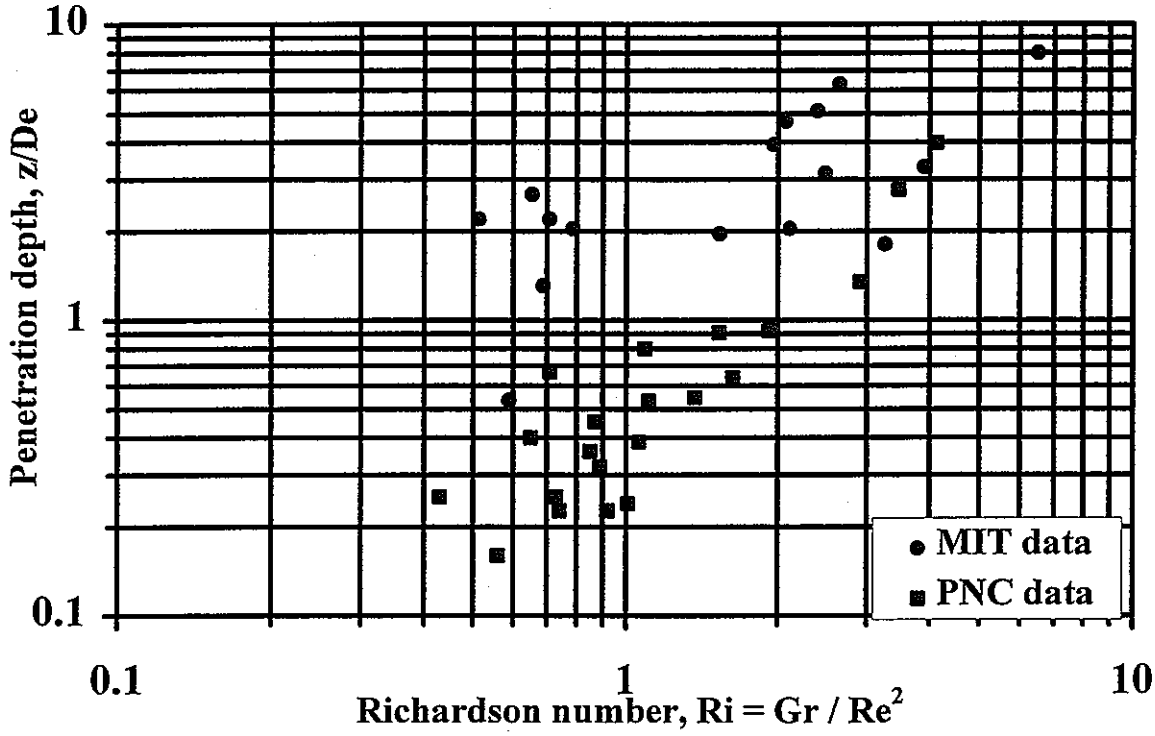

Figure 15. Penetration depth versus Richardson number. Present data and data extracted from Barakat and Todreas.

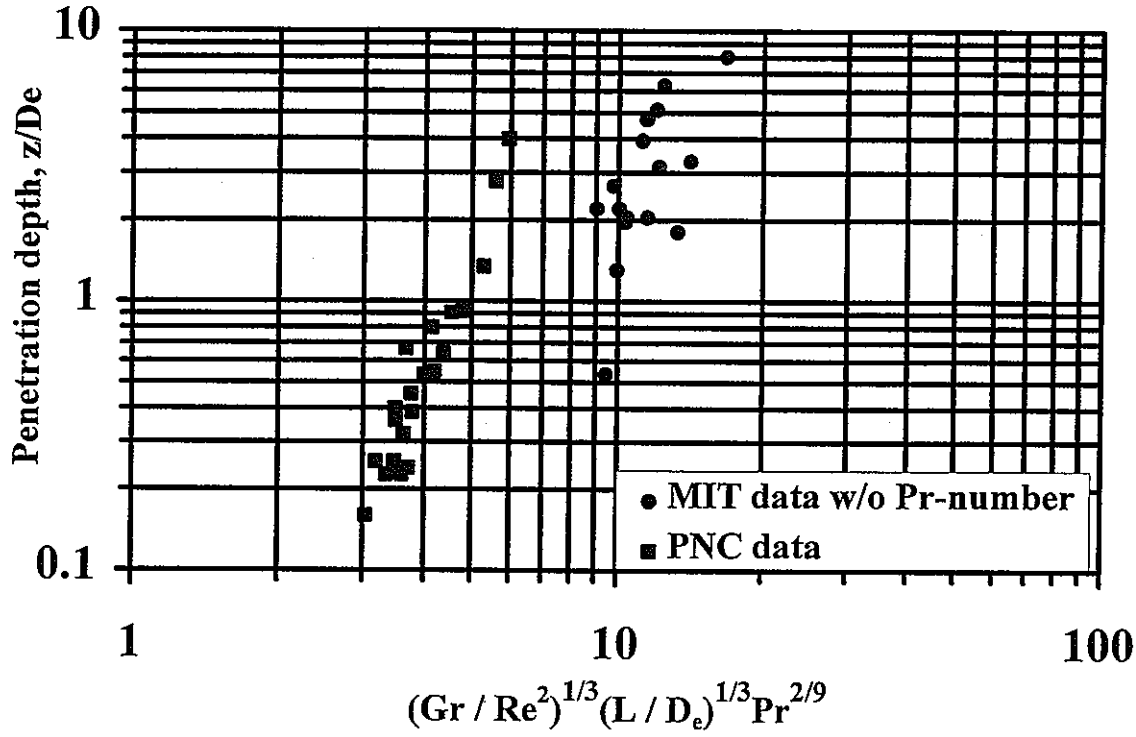

Figure 16. Penetration depth versus the new grouping $(Gr / Re^2)^{1/3}(L / D_e)^{1/3}$

The Prandtl number factor, $Pr^{2/9}$, is included in the present data.